2023

A Novel Unidirectional Smart Charging Management Algorithm for Electric Buses

Nicolae Darii

Roberto Turri

Keith Sunderland

See next page for additional authors

Funder: This research received no external funding

Authors
Nicolae Darii, Roberto Turri, Keith Sunderland, and Fabio Bignucolo

electronics

MDPI

Article

A Novel Unidirectional Smart Charging Management Algorithm for Electric Buses †

Nicolae Darii [1,*], Roberto Turri [1], Keith Sunderland [2] and Fabio Bignucolo [1]

[1] Department of Industrial Engineering, University of Padova, 35122 Padova, Italy
[2] School of Electrical & Electronic Engineering, Technological University Dublin, D07 EWV4 Dublin, Ireland
* Correspondence: nicolae.darii@studenti.unipd.it
† This paper is an extended version of our paper published in 57th International Universities Power Engineering Conference.

Abstract: The difficulty of controlling the charging of electric buses (EBs) and their effects on network demand are discussed in this study. The solutions suggest a call for worldwide, complex infrastructures that manage EVs and EBs equally. Additionally, the Distribution Network (DN) must be prepared for an increased prevalence of reverse power flow caused by widespread distributed renewable generation. This paper focuses exclusively on EBs since they have higher capacity and predictable charging patterns, which makes them more significant for the DN in the context of a transition to complete vehicle electrification and technologies that are mature enough to be hosted. The proposed algorithm employs the Day-Ahead Energy Market (DAEM) in the Smart Charging (SC) to forecast the network operating circumstances. Additionally, the technique makes it possible to facilitate distributed photovoltaic (PV) generation, allowing network demand to be referenced depending on net demand. It also identifies an appropriate individual charger current per vehicle and per-time-step with load-levelling or peak-shaving as its primary goal. The final real demand demonstrates that a coarse correction of the demand is possible. According to the analysis of the DN voltage profile and associated line losses, the ideal node position location of the CS is dependent on PV penetration.

Keywords: electric buses; distribution network services; charge management algorithm

Citation: Darii, N.; Turri, R.; Sunderland, K.; Bignucolo, F A Novel Unidirectional Smart Charging Management Algorithm for Electric Buses. *Electronics* **2023**, *12*, 852. https://doi.org/10.3390/electronics12040852

Academic Editor: Nikolay Hinov

Received: 9 January 2023
Revised: 5 February 2023
Accepted: 6 February 2023
Published: 8 February 2023

1. Introduction

A major contribution across several sectors is required in the context of the general transition to greener economies and smarter technologies. Transport and energy, for example, account for 63% of worldwide CO_2 emissions [1]. Furthermore, there is an official obligation to attain Net-Zero-Emissions by 2050 in order to limit global warming to 1.5 °C [2]. These demands coexist with a rapidly increasing electrification of the automobile sector and an increase in distributed and centralized renewable generation. As these actors must be introduced into the electricity distribution system (Distribution Network (DN)) if an energy transition strategy is to be realized, the question arises of whether the distribution network is prepared to host them. Indeed, an uncontrolled introduction could have an impact on how the network operates. As a result, there is considerable study interest in appreciating solutions that handle the incorporation of Electric Vehicles (EV) and Renewable Distributed Generation (RDG) [3–5]. Vehicle-to-Grid (V2G) systems, Smart-Grids (SG), and Internet-of-Things (IoT) are examples of advancements that facilitate and manage these elements. These new paradigms arise as fresh solutions to looming needs. These proposals are often characterized by a high level of complexity, necessitating the use of technologies, such as a capillary communication infrastructure, to maintain real-time control. Furthermore, the DN, where EVs and RDG will be prevalent, will require a radical intervention to be able to host forecasted EV and RDG expectations [6].

These factors necessitate for improved implementation in transportation infrastructure and electricity networks to be prioritized if climate change timelines and technology integration goals are to be realized. As a result, a greater study effort is required to comprehend the aforementioned (technical) issues associated with V2G in the context of the technical restrictions of the (DN) and the regulatory aspirations set by governments. Moreover, modelling V2G with an emphasis on public cars, using an approach that does not require extreme measurement system modifications, could also align with Government goals. The focus of this study was on public EVs, notably Electric Buses (EBs). The technology could be applied to other types of electric vehicles that are expected in communities, such as municipal refuse trucks or school buses. Iclodean et al. claim that public EV will be the first prospective users of a V2G service [7]. The complete deployment of private EVs for V2G prospects has various hurdles, including an effective economic reward system, more robust demographic research and appreciation, and user behavior (including variables such as "range anxiety", etc.) [8]. EBs avoid such 'difficulties'. They are supported by the government, and as stated by P. Yannick et al. an EB storage system is distinguished by the enormous capacity of the batteries and their standardization potential. Furthermore, public EBs are governed by timetables, which may eliminate the (utilization) unpredictability that characterizes private EVs. Prioritizing public EBs in the development of a V2G service is expected to have the effect of incentivizing the transition to greater integration, which could also support private EV with an overall impetus to encourage more renewable RDG opportunities [9]. It has also been shown that public EBs can recoup their capital expenditures by providing an energy (capacity) service during peak demand hours [10].

According to Uddin et al. [11], three primary methods are currently available to control the electrical demand: the use of Battery Energy Storage Systems (BESS), Demand/Response (DR), or the management of Electric Vehicles (EV). The management of the EV, is currently not feasible due to a lack of vehicles and infrastructure to provide an adequate service. However, the number of EV sales shares in the Net Zero Scenario (NZS) is expected to expand exponentially [12], implying that there will be a significant amount of energy to manage (EV, in this regard, count as load and storage). Peak shaving and load levelling may be accomplished by cleverly charging the vehicles ("Smart Charging" techniques) to achieve the desired load at the grid side, while concurrently charging the vehicles from the consumer/load side. This method has significant drawbacks as well however, because EVs are only active on the grid while parked. A single car has little effect on the load side, and charging synchronization is a difficult operation because it is dependent on the user's unpredictable behavior. Controlled charging infrastructures are scarce, and developing them in metropolitan areas is particularly difficult. This offers further justification why the research presented here concentrates primarily on EBs to facilitate V1G (or Unidirectional Smart Charging), because V1G has the potential to overcome capacity, scheduling, and cost issues. Even though the IEA stated in [13] that there will be less than 11% EB stock in the world by 2030, the trend for urban areas suggests the contrary. In order to progress towards more environmentally friendly scenarios, some major cities, as discussed in [14], have already begun to transition to (mostly) "car-free" cities and to migrate to public transportation systems. In this regard, EBs offer a peak shaving or load levelling service, which might be included in an Ancillary Service Market or subsidized by the Government to make it competitive and easy for the CS [15]. This study, which is an expanded version of our work that was published at the 57th International Universities Power Engineering Conference [16], concentrated on a Smart-Charging (SC) algorithm that makes use of demand data from the Day-Ahead-Electricity-Market (DAEM). The algorithm provides a Load Leveling or Peak Shaving service by managing the current absorbed by each EB in a Charging Station (CS), while satisfying the charging requirements of the EBs and adhering to a reasonable connection pattern defined by the fleet limit of the EBs.

2. Materials and Methods

2.1. Single Battery Modelling

Batteries are at the core of the CS system and this component plays a strategic role in the EV field. Therefore, there is a plethora of studies on the topic [7,17–19]. Some of the technologies employed include: Molten Salt (Na-NiCl2), Nickel Metal Hydride (Ni-MH), Lithium Ion (Li-Ion) and Lithium Sulphur (Li-S). In the study undertaken by Iclodean et al. a comparison among different type of batteries applied on the same vehicle is considered. The most commonly used commercially is the Li-Ion battery [7], which has a small "memory effect" that reduces the initial capacity over time. Even though the energy density is higher, the tests demonstrated that, for the same conditions, the Li-Ion has less autonomy (battery duration at a specific load level) than Ni-MH, which are the also widely used because of their high energy/power density. Li-Ion is currently the most convenient battery technology, even with the associated strong drawbacks related to the autonomy and temperature sensitivity. Further, due to the fact that 25–50% of the entire cost of an EV concerns the battery, it is essential to be cognisant of the associated implications. In the context of a potential fast transition to EV, it is compulsory to implement technologies that are economically competitive in order to incentivize such transition. Consequently, the battery type that has been taken into account in this work is the Li-Ion since it has a strong competitive price and it is the battery technology that applies most satisfactorily to the relevant (technology) transition considerations. The Li-Ion batteries can be controlled by adjusting: voltage, current, temperature and the load supplied by the battery. As suggested in [20], this makes them suitable for electrical vehicles and grid applications. Generally, the most important functions that define the state of the battery are Equations (1) and (2):

$$SoC_{\%} = \frac{1}{(C_r V_r)} \int_0^t i(\tau) v(\tau) d\tau \tag{1}$$

$$v = f(SoC_{\%}). \tag{2}$$

Among the different typologies to model battery effects, the most suitable for EV's applications is the Equivalent Circuit Method (ECM). This method uses lumped electrical components and controlled voltage sources in order to model the battery's physics and chemical reactions, therefore it is possible use to electrical circuits solvers, in particular the one suggested by Tremblay in [10]. This model has the peculiarity that requires just three points from the manufacturer's discharge *SoC*-Voltage curve to obtain the parameters. In addition to this, the SIMULINK^{TM} software uses this model in the SimScape library as the battery. This model is characterized by two components: a fixed internal resistance R_{int} that models the complex physical and chemical reactions that causes voltages drop and heat (modelled as Joule Effect). The latter is an ideal controlled voltage generator that represents the V_{oc} (Open Circuit Voltage) of the battery as presented in Equation (3). An extraction of the battery modelled characteristic is contained in Table 1, starting from the battery's rated capacity and voltage. Zhang X et al. considers an ECM model that has some limitations [21]. It is necessary to be aware of the hypothesis used by the model in order to not overestimate the results of the algorithm. For the work presented here it is important to consider how the voltage behaves during the charging pattern because it is focused only on the unidirectional smart charging process. In order to compute the actual energy that is stored in the battery, it is necessary to know the voltage at the terminals as it is possible to see in Equation (1).

Table 1. Parameters Tremblay's Equation.

$E_0[V]$	$R[\Omega]$	$K[\Omega, V/(Ah)]$	$A[V]$	$B[Ah]^{-1}$

$$V_{batt} = E_0 - R \cdot i - K\frac{Q}{Q - it} \cdot it - K\frac{Q}{it - 0.1 \cdot Q} \cdot i + Aexp(-B \cdot it). \quad (3)$$

Li-Ion batteries are extremely sensitive to temperature [22]. Frequent charge/discharge cycles also decrease the life cycle of the batteries [23,24]. In addition, the internal resistance changes over time when the internal structure of the electrodes changes. The effects are more intense when the batteries are operating at high C-rates (the unit used to measure the speed at which a battery is fully charged or discharged). To avoid the aforementioned adverse effects caused by the fast charging, it is common to restrict the battery's operation at their nominal C-rate, however Amietszajew et al. proved that it is possible to use the cells in a wider C-rate range [15]. Since the batteries of an EV could be solicited to employ higher currents (for example, an EB), it is necessary to know the *SoC*% range that could resist fast charging. The first safety limit is to impose a lower limit on the *SoC*, since the voltage will drop drastically when the *SoC* is close to the lowest tolerable value, for instance, an *SoC* of 20%. When the battery reaches the highest values of permitted *SoC*, the internal resistance R_{int} of the battery tends to grow, increasing the over voltage, Joule Effect would result in a degradation of the cathode. Therefore, a safety limit is imposed for a *SoC* of 80% to limit the temperature, lithium planting and extreme polarization (which causes a voltage spike when the $SoC \cong 100\%$). This is why a high Constant-Current (CC) charging for an *SoC* of less than 80%, and a Constant-Voltage (CV) charging with *SoC* greater than 80% are adopted in fast charging techniques. Even if this is the most common charging protocol, it is also the least time-efficient. The possibility of charging the batteries at higher rates when $20\% \leq SoC \leq 80\%$ is suggested by Amietszajew. To achieve a safe charging pattern, it is not necessary to impose a gradual reduction of the C-Rate, as the current magnitude will follow the Load demand, which increases and decreases naturally and gradually. In addition, outside the periods where there is an under load demand (and for high currents to facilitate some compensation), the charging current is less than or equal to nominal.

By considering just the polarization effects of the Tremblay model, a test on the voltage increase of a Li-Ion battery pack with 650 V as rated voltage, 660 Ah capacity Q and a charging current of 600 A was carried out. As the polarization effect is proportional to the current Equations (4) and (5), it was selected as the worst case in order to verify the discrepancy between the rated and distorted voltage.

$$V_{V.Pol} = K\frac{Q}{Q - it} \cdot it \quad (4)$$

$$V_{R.Pol} = K\frac{Q}{it - 0.1 \cdot Q} \cdot i. \quad (5)$$

The result appreciable in Figure 1 shows that the divergence of this voltage during the charging pattern is not significant since it is less than 5 V (0.77%) in the range bounded between 20% and 80%, demonstrating that it is possible to use the rated voltage curve as a reference. In addition, there is the possibility to consider the voltage constant during the charging process as the error incurred can be neglected. For a more qualitative result, the algorithm employs a (MATLAB^{TM}) polyfitted Voltage characteristic that is a function of the *SoC* for more precise results when the battery is close to 80%.

2.2. Single Charger and Linearization

The charger choice has an important influence on how the batteries are employed. The first difference is the possibility to have either an internal charger (On-Board Charger, in practice a controlled rectifier) in the EBs or one that is accessed externally [25]. This method is adopted primarily in private EVs that have to be charged in domestic environments by connecting the EV directly to a low voltage AC supply via a plug-in receptacle [26]. Therefore, the capacity of the internal charges are limited to small powers/capacity and it is not possible to have external control because the vehicle self-modulates the power according to its charging protocol. For the purposes of this paper, there will be an emphasis

on external chargers, which are primarily connected to a Charging Station (CS). This charger typology can facilitate more power, and use higher voltage levels to reduce the current magnitude, and as a result, the associated charging losses.

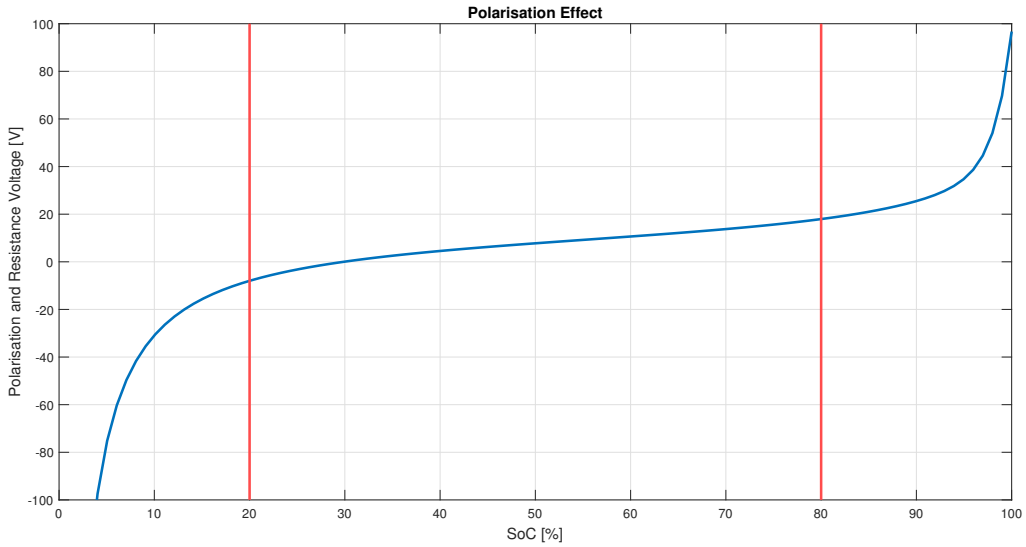

Figure 1. Limited polarization effect between 20% and 80% SoC

There are two possibilities associated with external chargers and their control typologies. The first employs a combination of an inverter and a DC-DC converter per vehicle. The alternative one employs a DC-DC per vehicle to connect all the converter primaries to a common DC-Busbar and then a single larger inverter connects the vehicles to the grid. The first method is mostly for isolated charging columns and has the peculiarity of a relatively small inverter size. The typology is useful when there is the possibility to combine a small size of renewable distributed generation, with an EV. By controlling the DC-DC and the EV's inverter, it is possible to track the power from the RDG (for example a domestic PV generation) and compensate for the power produced to absorb more uniform power from the distribution network [27]. The effectiveness of this method depends on the quality of the power tracking system and the coordination between all the vehicles connected to the specific node.

As the number of vehicles supplied by the same CS increases, the coordination of the DC-DC and inverters becomes more complex, and the second configuration, as depicted in Figure 2, is preferable, where the RDG is connected to the AC side and the vehicles are all controlled with DC-DC converters and then connected to the AC grid with a single inverter. With the second configuration, it is possible to modulate the current absorbed by each EV by controlling the DC-DC converters and then by regulating the larger inverter capacity to the grid's requirements. The coordination in this case is simpler, but it is necessary to rely on a more expensive inverter. Moreover, there is no redundancy if the inverter becomes out-of-service. Since the energy that an EV could exchange is limited, the service provided in this approach is more effective as "Power intensive" rather than "Energy Intensive", to accommodate any power fluctuations. The instantaneous value of the power generated by the RDG has to be tracked and communicated rapidly in order to have an effective control over the devices. Even if studies like [27], proved the effectiveness of the method, the technology required is not yet available and the DN is not ready to host proficiently this type of service. Therefore, since the goal of the present study is to focus on a technique that is easily accessible from a technological and management perspective, mono-directional power-flow is prioritized. In this regard, the choice of the DC-DC converter could be further discussed in order to obtain a more efficient and economical service. The bi-directionality of the half-bridge is possible with the introduction of more components rather than a DC-DC Buck or Boost [28]. Thereby, the efficiency is sacrificed in order to obtain a bi-directional

power flow, which is not a requirement for the algorithm proposed here. So a DC-DC Buck converter is preferable both in terms of its efficiency (cost, complexity) and operability in the context of the inevitable time available before a full transition involving the full range of communications control is available.

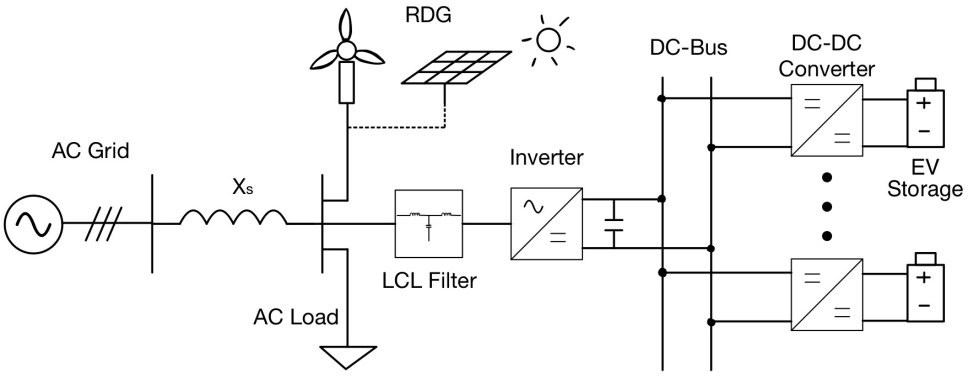

Figure 2. Schematic EV DC-Bus [27].

The other problems involving EVs and the CS, include the uncertainty of the EV's parking pattern; plugging problems; different typologies and sizes of the batteries, etc. [27]. These aspects add randomness to the EV's charge planning and management. EBs have: higher battery capacity, same size and typology, scheduled mission. These characteristics lead to a relatively higher involved power, the elimination of the diversified approach based on vehicle's model, and a reduction in the randomness of the charging pattern. In order to have simpler relationships that involve constant parameters in the relative time-frame, it is necessary to modify the behavior of the inputs in Equation (6).

$$E[Wh] = \int_0^t i(\tau)v(SoC(\tau))d\tau. \tag{6}$$

Since the batteries are usually used in CC mode in the fast charging range, Equation (1) can be expressed without the voltage terms and if the current is considered constant with discrete time steps, it is possible to simplify the *SoC* expression as Equation (7). Subsequently, since this *SoC* formulation is related to the [Ah] unit of measurement, it is necessary to modify it in terms of energy in [Wh] to facilitate a comparison with the data from the DAEM. To do so Equation (2) and more specifically the spline poly-fitted function, is employed. Therefore, energy, as described in Equation (6), becomes Equation (8).

$$SoC_{\Delta t} = \frac{I \cdot \Delta t}{C_r[Ah]} \cdot 100 \tag{7}$$

$$E[Wh] = \frac{SoC \cdot C_r[Ah]}{100} \cdot V(SoC(I)). \tag{8}$$

With a view to achieving a process linearity in terms of power transfer, as it facilitates the EBs to be operated separately while still having a unified end impact on the final CS's power, it is more useful to exploit the analytical expression to facilitate a forecast of the actual energy on subsequent discrete time steps. With Equation (9), it is possible to find the new *SoC* level and the linearity of the formulation is clear. The computation of the new charge level is more accessible in *SoC* form, as provided in Equation (10).

$$SoC_{t+1} = \left(\frac{100 \cdot V(SoC_t) \cdot \Delta t}{C_r[Ah] \cdot V_r} \cdot\right) I + SoC_t \tag{9}$$

$$E_{t+1}[Wh] = E_t + \frac{SoC_{t+1} \cdot V_r \cdot C_r[Ah]}{100}. \tag{10}$$

The application of Equation (9) has been verified by simulating the charging process and including the Buck Converter's switching effect, with different constant currents to confirm the linearity with a model built in SIMULINK^{TM}. By controlling the current with different values, the power, as illustrated in Figure 3, and the energy, as portrayed in Figure 4, at the DC/DC Buck terminals, follows a relatively linear and 'constant' pattern that is proportional to the current's magnitude including the additional implications caused by the Buck's switching.

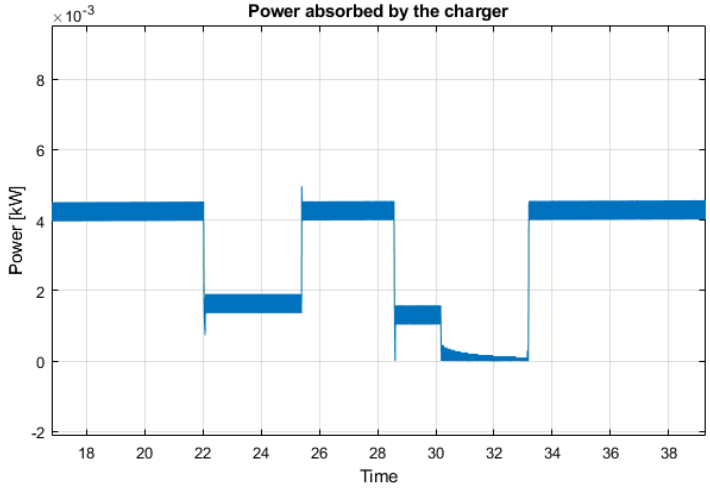

Figure 3. Buck converter power

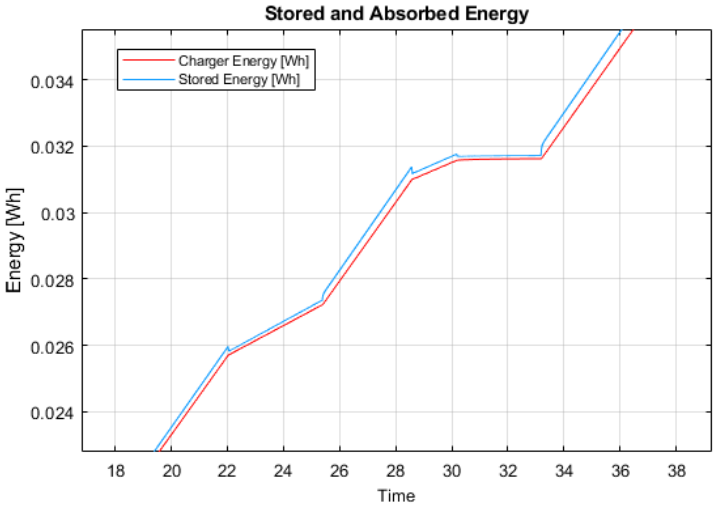

Figure 4. Buck converter energy.

In conclusion, the approach advocates for linear relationships in the consideration of battery energy and *SoC*. In achieving this approach, a more complex model that includes the polarization effects, can adopt a linear energy/power with a step-wise current pattern, if the battery operation is restricted within the 20–80% *SoC* range. Consequently, it is possible to associate the current and power quantities through suitable vectors (developed in MATLAB^{TM}) and compute the current required. This approach facilitates the opportunity to test iteratively the energy to be provided to the EBs in the time step $t + 1$ until the entire energy of the whole CS matches the one required to improve the DN demand's shape.

2.3. The Functionality of the Smart-Charging Algorithm

Some methods for managing electric buses or charging stations can be found in the literature. Zhuang P. and Liang H. proposed a stochastic method [29], Han B. et al. a

method that uses timetables and routing as constraints [30], and Hasan M.M. et al. a method that improves electric motor efficiency [31]. Gkiotsalitisin K. emphasized the necessity of regular charging periods for EBs in lowering passenger travel time [32]. Zhang C. proposed a strategy for overall optimization of EB scheduling [33].

The algorithm presented in this study intends to propose a solution that may be employed in a smart grid transition by leveraging readily available data (DAEM, datasheets, etc.) to construct a CS load profile and the EB scheduling, to achieve a given demand shape in a restricted DN. Furthermore, exact currents and EB schedules are prepared every 15 min for general CS management purposes.

On the other hand, the algorithm could be used to forecast the effects of a given CS and EB on different DN configurations (loads, PV, etc.). It allows for the photovoltaic (PV) power and the penetration of self-consumption (allotment of PV power saved in batteries during the day to be used during the night to reduce power absorbed by the grid) to be altered. To simulate alternative scenarios, the quota of the PV installed in the DN and the self-consumption as a proportion of its rated installed power can be changed. As the generated PV power saved for local consumption is not part of the usual load, it reduces the PV curve magnitude, thereby mitigating the Duck Shape (a sinking impact of the demand shape during the noon hours caused by increased PV generation, resulting in lower grid energy demand) [34]. The load is further decreased during the hours of darkness, when demand is already low. Furthermore, the produced power can be adjusted from 0 to 100% of the rated PV output to simulate varied weather situations.

The first operation is to polyfit the original demand curve in order to obtain Equation (11). The algorithm requires the target level for the relevant day, which could be partial peak- shaving or total load-levelling, and produces a vector containing the objective demand per time step, $\mathbf{P}_{objective}$. The $\mathbf{P}_{objective}$ vector is in discrete form, to compare the actual demand with the objective, and Equation (11) is discretized by computing the average power in a $\Delta t = 0.25[h]$ time period, consistent with how DAEM is presented. Thereafter, the equation represents its vectorial form $\mathbf{P}_{load}$.

$$\mathbf{P}_{load} = f(t). \tag{11}$$

Thereafter, the energy difference between the actual demand and the aim is estimated for each time step i long Δt, resulting in the $\mathbf{E}_{load}$, Equation (12) with $n = 24[h]/\Delta t = 96$ elements. The power absorbed by the charging station will be already incorporated in $\mathbf{P}_{load}$ by taking into account each EB continuously absorbing the rated current I_r. During the $\mathbf{P}_{objective}$, however, the vehicles will absorb a "smart current" I_s based on their $SoC\%$ status. The algorithm applies I_r, the current to each EB j at each time step by computing the new SoC with Equation (9) and then translating it to [kWh] with Equation (10) to acquire the energy $E_{j(r)}$. To start the smart charging process, the initial current $I_s = 0$ is enforced to produce $E_{j(s)}$. Then, in order to compute the difference in energy between the normal operation and the smart process, the full CS's energy transition with all m EBs is expressed in Equation (13). The EBs will be charged with the same I_s during the smart charging process, with the exception of vehicles that, if charged with I_s, would exceed the $SoC = 80\%$. As a result, the smart current for these vehicles will be charged with a current I_e calculated using Equation (14).

$$\mathbf{E}_{load} = (\mathbf{P}_{load} - \mathbf{P}_{objective}) \cdot \Delta t, i \in [1, n] \tag{12}$$

$$\Delta E_{CS} = f(I_s) = \sum_{j=1}^{m} (E_{j(r)} - E_{j(s)}) \tag{13}$$

$$I_e = (80 - SoC_{\%}) \cdot \frac{C_r \cdot V_r}{100 \cdot V \cdot \Delta t}. \tag{14}$$

The algorithm will first calculate the energy for each EB in order to obtain Equation (13) for the i time step, and then the objective function Equation (15) will be tested. More

specifically, it is checked if the chosen current I_s achieves the correct reduction/increase in CS energy at time step i. If the criterion is not met, the process is repeated by increasing I_s by 0.1A until the condition is fulfilled. The SoC_{i+1} generated by Equation (9) is then assigned to SoC_i for the next time steps $i+1$, and the method is continued until the last time step $i = n$ for each element of $\mathbf{E}_{load}[i]$. Figure 5 illustrates that it is the rise/reduction of energy between each time step that affects the ultimate load form, and not the energy already stored in the vehicles. In Figure 5 case, $I_s > I_r$ with $\mathbf{P}_{load}[i] \ll \mathbf{P}_{objective}[i]$, therefore the vehicles start at a specific SoC% represented in yellow, the orange increment represents the additional charge that should be achieved if the vehicles were charged with rated current I_r. Thus, the blue level represents, in this case, the one that is required in order to achieve the DN requirements by charging the EBs with the smart current I_s (the initial demand lower than the required one).

$$\Delta E_{CS}(I_s) - \mathbf{E}_{load}[i] \leq 0. \tag{15}$$

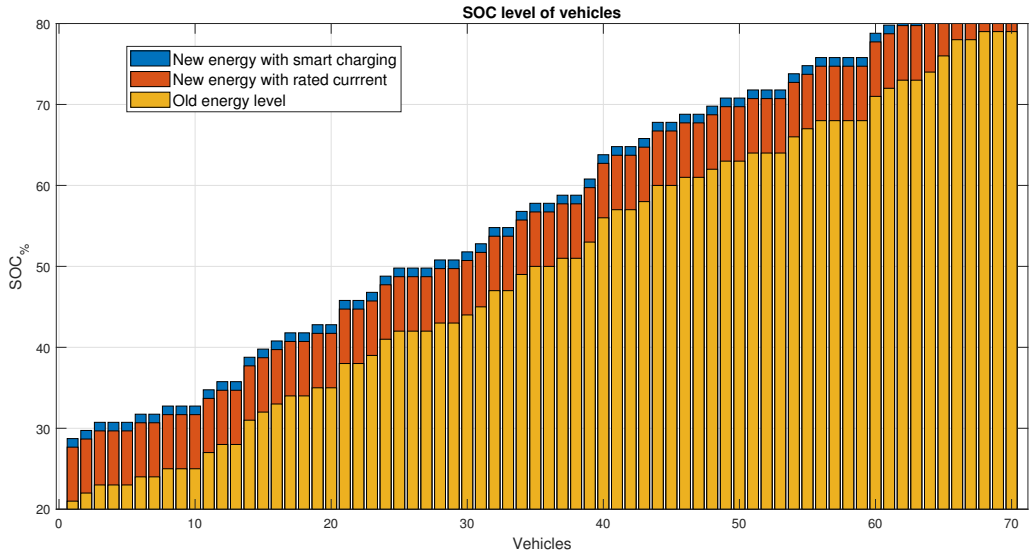

Figure 5. EBs SoC at time step t and t + 1.

The smart current will have four cases as in Equation (16). The case that could present difficulty is when the difference between the demand and the objective power is greater than the one that achieves the proper CS ($\mathbf{P}_{load}[i] \gg \mathbf{P}_{objective}[i]$). In such a case the algorithm imposes $I_s = 0$, so it turns off the entire CS and reduces the load as far as the CS can.

$$\begin{cases} \mathbf{P}_{load}[i] \gg \mathbf{P}_{objective}[i] \Rightarrow I_s = 0 \\ \mathbf{P}_{load}[i] < \mathbf{P}_{objective}[i] \Rightarrow I_s > I_r \\ \mathbf{P}_{load}[i] > \mathbf{P}_{objective}[i] \Rightarrow I_s < I_r \\ \mathbf{P}_{load}[i] = \mathbf{P}_{objective}[i] \Rightarrow I_s = I_r \end{cases} , i \in [1, n] \tag{16}$$

The $\mathbf{P}_{load}[i] \ll \mathbf{P}_{objective}[i]$ example could take a long time to compute because the current only grows by 0.1A per iteration until it reaches the correct value or the maximum eligible current. To improve this issue, an adaptive current increment could be employed. The last unmarked instance with $I_s < 0$ might be implemented with a DC/DC Half-Bridge and is thus ignored. As a result, the currents (I_s, I_e) and SoC% are saved in Equation (17) for each iteration at step I for each EB j. Vehicles that achieve $SoC = 80\%$ at time step i are then connected with vehicles that achieve $SoC = 20\%$ at $i+1$, which is considered the best situation.

$$\mathbf{SoC}_{\%}[j, i], I_s[i, j], i \in [1, n]\ j \in [1, m]. \tag{17}$$

The tracking of vehicles that reach $SoC = 80\%$ is recorded in a vector **Cnn** Equation (18) that contains the number of EBs that have reached the limit, $z_i < m$. The entire fleet is

then computed using Equation (19) to achieve perfect load levelling. The **Cnn** vector is used to create the time slots represented by the bars in Figure 6, where the vehicles must be connected in order to have the sufficient power in the CS for the DN's load-levelling. There is a need to have more EBs available to connect during the time steps where the number of ideal exchanged vehicles is higher. In general, Equation (19) will generate numbers that have no physical or economic meaning (e.g., 70 EBs in the CS with a total fleet of 1000 EBs), hence the value is normalized by inputting the actual size of the available fleet. At this point, the method assigns the real number of EBs uniformly in the **Cnn** slots and generates the $\mathbf{Cnn}_{real}$ Equation (20) vector, which will include $z'_i \leq z_i$ EBs as elements, with the remainder set automatically in idle mode ($I_s = 0$) by Equation (14).

In reality, some EBs with $I_s = 0$ will remain in the CS as there will be a practical constraint in the limitation on the number of EB available to exchange; however, vehicles in idle mode (with $SoC = 80\%$) will be able to begin their mission. In other words, it is not necessary to have m vehicles in the CS at all times. This vector might be used to build the CS timetables, and it is possible to see graphically which time steps are most relevant to actuate the exchange, in order to synchronise the mission with the electrical demand needs (as illustrated in Figure 6). The blue bars in Figure 6 appear only in some time steps and show the number of vehicles z_i that must be connected at time step i in order to achieve an appropriate load-leveling (within the CS's power restrictions).

$$\mathbf{Cnn}[1, n] = [z_1, z_2, ..., z_n] \tag{18}$$

$$F_{ideal} = m + \sum_{i}^{n} \mathbf{Cnn}[i] \tag{19}$$

$$\mathbf{Cnn}_{real}[1, n] = [z'_1, z'_2, ..., z'_n]. \tag{20}$$

Furthermore, in order to avoid impractical connection patterns, the starting $SoC\%$ value must be accurately adjusted. If all of the EBs are set to $t = 0$ with a SoC of 20%, the connecting pattern will look like Figure 6, where the vehicles reach the $SoC = 80\%$ value at once as it is possible to notice from the few high blue bars.

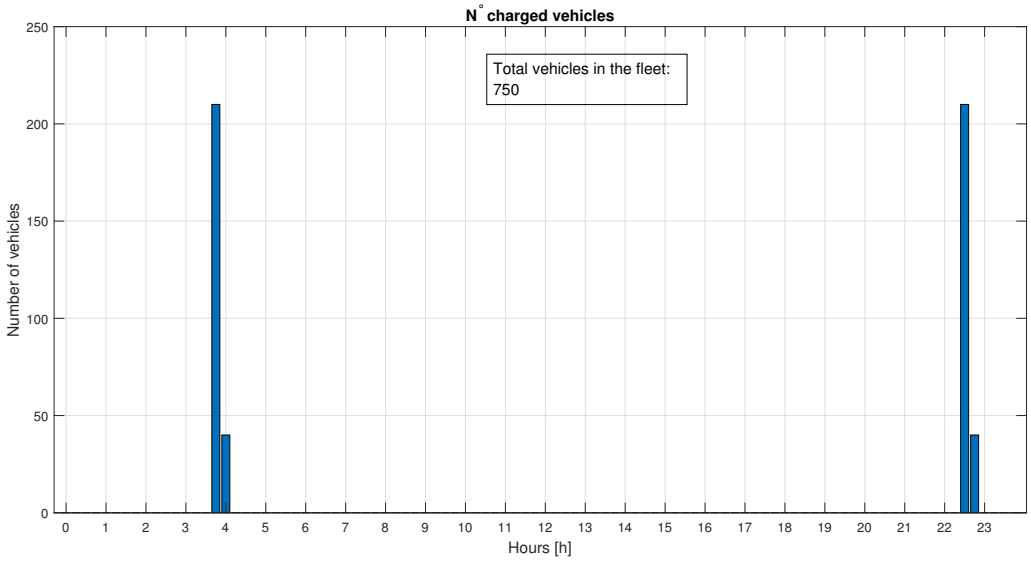

Figure 6. Connection with initial $SoC = 20\%$ for all EBs.

However, a uniform distribution of the initial SoC in the range of [20–80%] will yield a more realistic connection pattern (as illustrated in Figure 7) and produce an accessible connection pattern, as it possible to notice from the number and the height of the blue bars. Since the EBs are generally all charged with the same I_s, by imposing this initial condition, the number of the disconnected or connected ones are well distributed over 24 h.

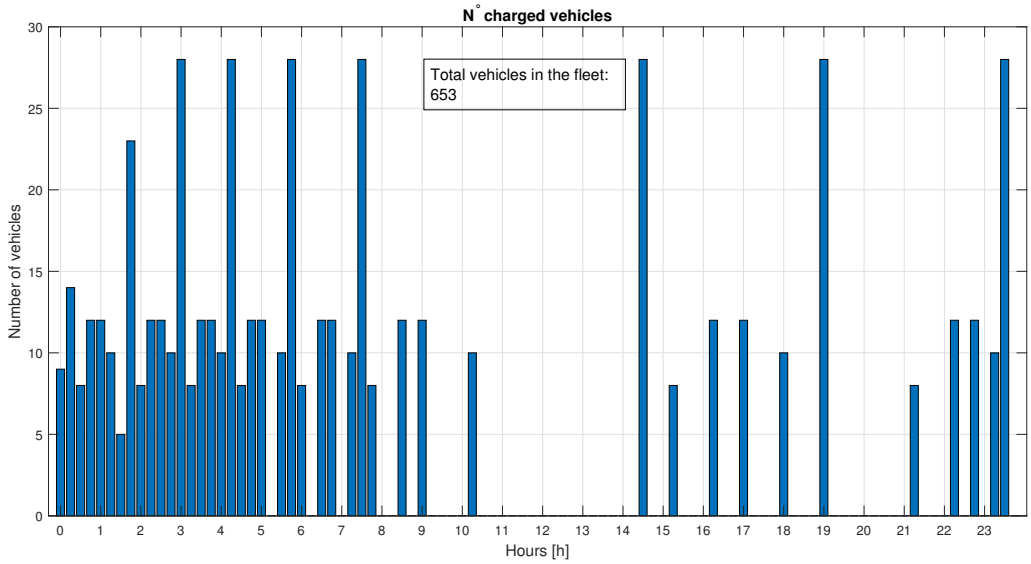

Figure 7. Connection with uniformly distributed *SoC*.

The ultimate mutual effects were computed in power terms and were compared to the starting power demand. Equation (21) computes the power $\mathbf{P}_{r(cs)}$ of the CS when the EBs absorb I_r, and Equation (22) computes $\mathbf{P}_{s(cs)}$, the total power absorbed by the CS with I_s. The final load was then calculated using Equation (23) and plotted to ensure the accuracy of the load levelling/peak shaving.

$$\mathbf{P}_{r(CS)}[i] = \frac{1}{\Delta t}\sum_{j=1}^{m}(E_{i,j(r)}), i \in [1,n] \tag{21}$$

$$\mathbf{P}_{s(CS)}[i] = \frac{1}{\Delta t}\sum_{j=1}^{m}(E_{i,j(s)}), i \in [1,n] \tag{22}$$

$$\mathbf{P}_{newload} = \mathbf{P}_{load} - (\mathbf{P}_{r(CS)} - \mathbf{P}_{s(CS)}). \tag{23}$$

Holistically, Figure 8 illustrates a representation of the whole algorithm in operation.

Color maps are another type of output produced by the method by utilizing the data stored in Equation (17). They are useful for providing a graphical global picture of the entire charging operation during a 24-h period. Looking at the current's color gradient can provide information on the DN's demand shape. The maps are generated from two matrices of size $[i, j]$, which may be transposed into EXCEL^{TM} tables to generate a charging pattern plan for each EB at each time step. A graphical depiction is required to have a global view of what is going on in the CS. Furthermore, the amount of the absorbed current can be shown to represent the influence on the network. The I_s matrix in the ideal scenario and the *SoC*%, with the charging current Is and SoC level (with the color) of each vehicle j at time step i.

Figure 9 depicts the illustration of Equation (14) when the EBs are nearly fully charged. For example, at the row corresponding to 4am, it is possible to see that the charging current is 140 A for most of the EBs. However, for the vehicles connected to the slots 20 to 50, the current color is different, therefore those vehicles are charged with a lower current (from 20 A to 120 A) because they are close to the full charged state. That is, for the precise vehicle j that will exceed the 80% *SoC*, the charging current will be tailored as I_e to achieve the exact full charge. The following square has the same color as the others since it represents a newly connected (discharged) EB that charges properly with I_s. Aside from the nearly charged vehicles, all of the others have the same charging current, which is why the color seems uniform during time step i. It is possible to note that the color does not vary monotonously

during the day, which is due to the network requirements: when $\mathbf{P}_{load}[i] > \mathbf{P}_{objective}[i]$, the indicator turns red (high I_s) and progressively turns blue (low/zero I_s).

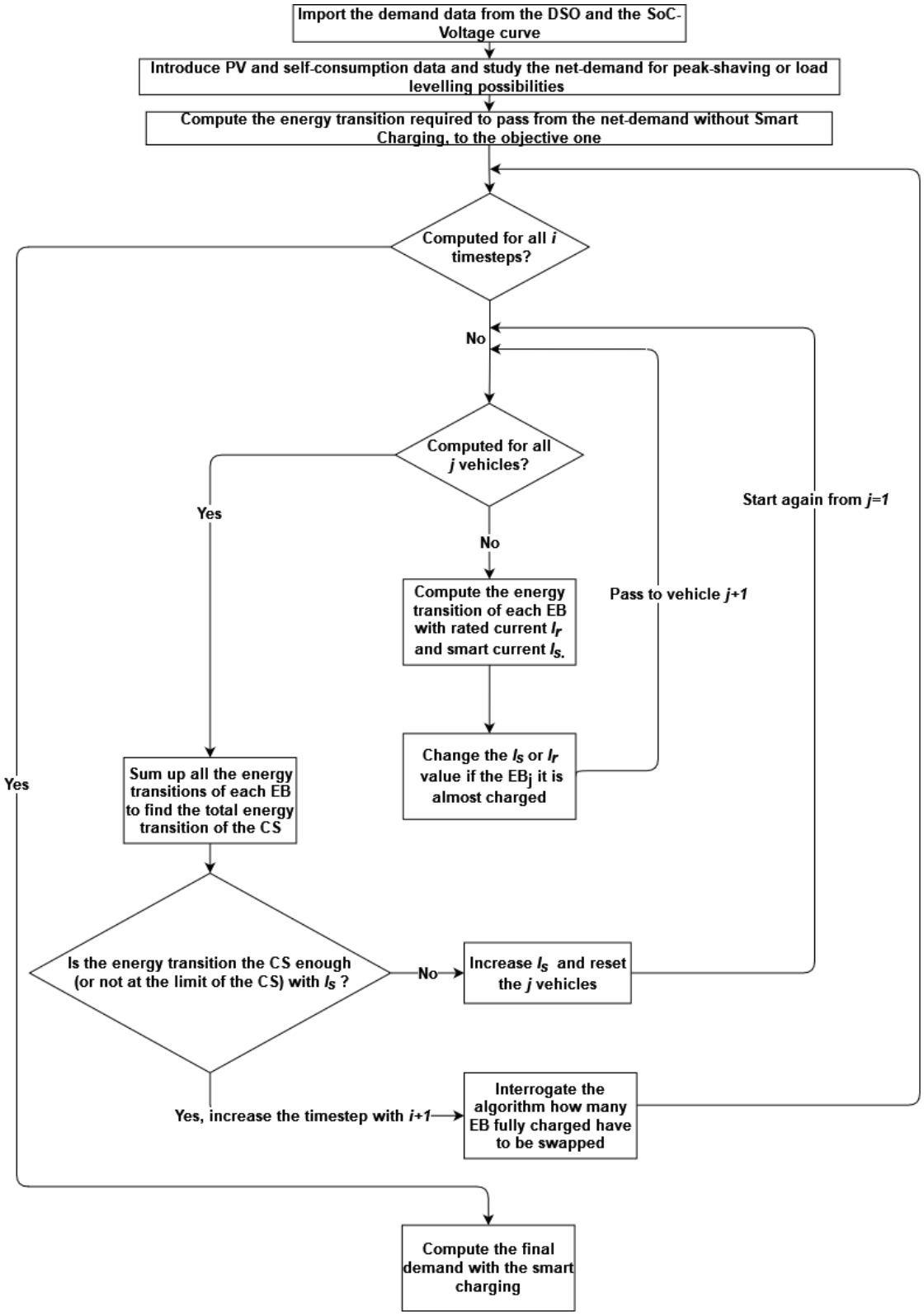

Figure 8. Algorithm flowchart.

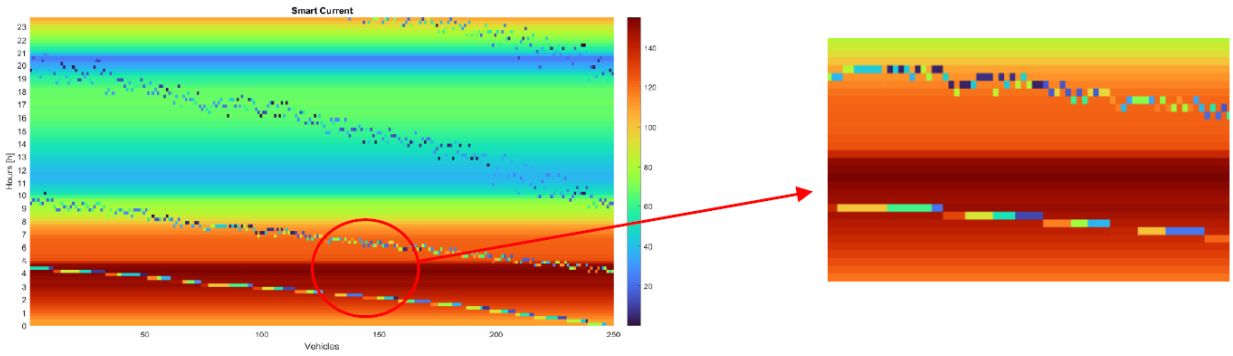

Figure 9. Zoom of the Currents I_e for the nearly charged EBs.

Since the current is represented in Figure 9 as a percentage of the $I_s / I_r \cdot 100$, there are some specific cases:

- Dark Blue when $I_s = 0$;
- Light blue when $I_s < I_r$;
- Green/Orange when $I_s \simeq I_r$;
- Red when $I_s > I_r$.

On the other hand, the *SoC* map Figure 10 can be used to depict the connection spots and the charging process velocity. When the gradient takes longer to transition from blue to red, the CS is absorbing less current, and vice versa. The map is handy for visually verifying the amount of time that the EBs would require to be fully charged by looking at the Δt between the top blue square and the last red square.

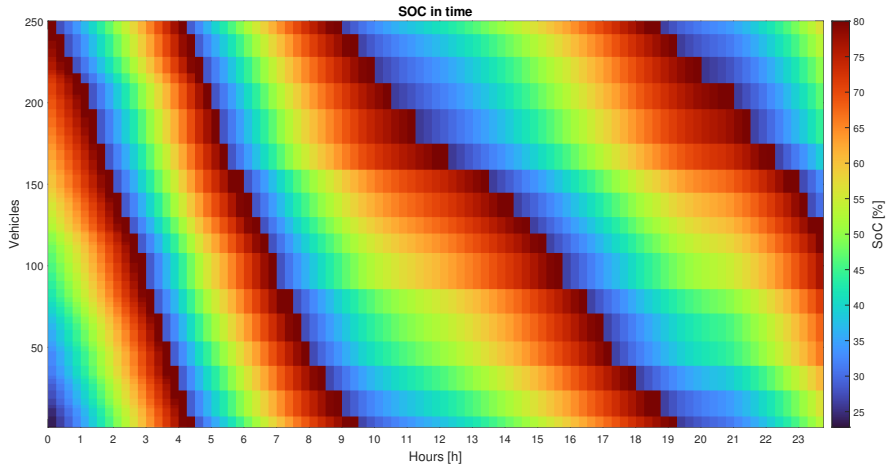

Figure 10. *SoC* color-map.

3. Results

3.1. Verification Criterion

As this article focuses on viable technologies, a standardized approach is required. This is also stated in [35], where Farzam Far M. et al. suggest that a standard approach is required to ensure a smooth transition in the increase deployment of the EB. The EB quota in 2021 was 4% of the global bus fleet and it is forecasted that it is necessary to have at least 20% of EB over the total fleet by 2030 in order to achieve the Net Zero Scenario [36]. This shows the necessity to have a common approach to incentivize the production of universal components and methods. At present there are numerous commercially available charging technologies that can be categorized as: conductive charging, wireless charging and battery swapping. As the latter two technologies do not currently have a market in Europe, the greatest solution for simplicity (both economically and constructively) is to

employ conductive approaches. The conductive chargers might be via Plug-In service or via Automated Connection Devices (ACDs), with the former being more suitable for small private vehicles with a power range of 60–150 kW and the latter being preferable for public EVs with a power range of 150–600 kW. The ACDs are categorized in the following ways: infrastructure-mounted (Type A), roof-mounted (Type B), and floor-mounted (Type C).

Although the European Parliament Directive 2014/94/EU (AFI Directive) provides some guidance for pricing infrastructures, there is (currently) no information relevant to EBs. This is critical, especially as EBs are expected to be the first actual user fully integrated into the electrical grid [9]. According to Farzam et al., there are programs such as ZeEUS (Zero Emission Urban Bus System) that aim to establish a standardization approach to EBs technology [35], and the CEN-CENELEC (European Committee for Electrotechnical Standardization) has begun to apply the ZeEUS recommendations. Another project is ASSURED, which attempts to create a common rapid charging strategy for all public vehicles (EBs, electric garbage trucks, delivery trucks, and so on).

The ASSURED project is a continuation of the ZeEUS project and is primarily concerned with the previously mentioned ACD charging techniques. There is also the ASSURED 1.0 initiative, which aims to develop an interoperability reference and test protocol for charging infrastructures [37,38]. The issue of safety is very important because EBs require more power than private EVs; hence, if a public infrastructure will enable EBs, it is crucial to be aware of a preferred technique to ensure operational safety. It is possible to receive information on what additional safety precautions are available that are purely focused on the battery [39,40]. Other components, such as the connection, are crucial because special care must be taken in the case of Plug-In services that come into touch with people during the charging process. For example, the SAE J1772 standard limits the use of connectors based on voltage type and magnitude as provided in Table 2.

Table 2. Chargers standards.

Charging Standards				
Level	**Type**	**Voltage**	**Current**	**Power**
1	AC	120 V	16 A	/
2	AC	208–240 V	80 A	19.2 kW
1	DC	50–1000 V	80 A	/
2	DC	50–1000 V	400 A	/

The article focuses on an ACD because of the enhanced performance (Type B). The voltage and current levels are higher in this case because of the increased demand for power from the EBs. Table 3 [41] of the IEC 68151 specifies the relative power, voltage, and current that an ACD "Opportunity Charger" can support. The Volvo Opp Charger and EBs as presented in Table 4 will be specifically considered in order to base the algorithm on practical and achievable values [42].

Table 3. IEC levels.

Output Requirements	
Power Levels (kW)	150, 300, & 450 kW
DC Voltage (V DC)	450–750 V
Frequency (Hz)	50/60 ± 2
Output Current (A)	0 to 200 A, 750 V, 150 kW 0 to 400 A, 750 V, 300 kW 0 to 600 A, 750 V, 450 kW

Table 4. Volvo Charger and EB [42].

Volvo OppCharger	
Maximum charging power level for EB (kW)	450
Output DC voltage (VDC)	500–750
Max output current at 750 VDC (A)	200/400
Ambient temperature (°C)	30
Volvo 7900 Electric Articulated	
Battery type	Li-Ion
Voltage (VDC)	600 V
Capacity (kWh)	264–396

As a comparative approach to verifying the algorithm's performance is not viable with the examples described in the literature aiming for different results, a separate criterion must be used. The strategy used in this paper involves several stages. To begin, EB and CS data that make physical sense are employed, but this approach will not always achieve optimal results. The first goal is to determine which scenario fits with a relative random EB and CS and to confirm that it fits with the tendency of the future DN's composition (moving towards DNs with prevalence of RDG and storage). The second stage prioritises the 'best' scenario to determine the most suitable configuration or the EB/CS (charging voltage, number of charging slots, fleet size, etc) and compare it to currently existing CS regulations in Table 3 and EBs in Table 4.

3.2. Ideal Scenarios

The algorithm can simulate how the DAEM demand would be affected if smart charging was enabled. Furthermore, the DAEM can be used to simulate various CS and network scenarios. It is also possible to create scenarios with varying RDG and storage levels. It is interesting to first examine how the CS and network respond to various RDG scenarios in order to determine the best charging condition in the ideal case and to confirm whether the algorithm produces meaningful values under different operational conditions. The ideal case assumes that as many vehicles as needed can be connected, so when a vehicle reaches $SoC = 80\%$, the next time step is changed to $SoC = 20\%$. This will produce an impractical fleet size. When a practical/plausible fleet size is imposed, the behavior will have a detrimental effect on the network. Therefore as an overview of the best-case scenario, a study of the ideal condition is considered and then by imposing practical considerations (such as fleet size) an analysis of more realistic network reactions can be considered for an enhanced assessment of network limitations. As the algorithm requires the ideal result in any case, studying scenarios with the ideal hypothesis requires half the computational effort, because a more realist appreciation of network performance based on the smart-charging of a practical EB fleet is achieved by a subsequent implementation of the algorithm. In other words, a more practical assessment involves two steps: an ideal charge management solution that is subsequently adjusted by a practical fleet size.

Three ideal scenarios will be considered: one without PV and storage, one with PV only, and one with PV and storage for self-consumption. For the test, CS and EB parameters that differ from those used by Volvo Table 4 will be used in the first stage, and a CS with poorer performance will be used. This is done to determine the convenient scenario for a CS with EB using a conservative technique that does not use the best CS and EB settings. The data from Tables 3 and 4 will be utilized as a benchmark in the second stage, where the goal is to determine which EB/CS values are the most appropriate. The test parameters are in Table 5, where the voltage is lower than the higher one in Table 3 to verify how much the EBs would be stressed on the current side. The P_{PV} is the installed power of the PV, which is modulated to simulate a cloudy day during the no-PV scenario. The $P_{Self\%}$ is considered as quota of the installed PV, which has a mutual effect on the power produced by the PVs. The energy used to charge the storage for the self-consumption is a quota taken from the PV's

production that will not satisfy the demand, therefore if the self consumption is included, the power available from the PV is lower. The self-consumption is hypothesized as being available during "dark hours", i.e., when the PV's output is zero. The ultimate goal of each scenario is to achieve a load levelling at an average level between the highest and lowest peak, therefore with a constant power of 25MW for 24 h. The summary of the all cases is presented as a review in Table 6 where different objectives and the relative outcomes are outlined. More specifically, the best scenario goal is one that seeks to validate how the DN responds to a CS and whether the most appropriate scenario is consistent with the real future DNs.

Table 5. Scenarios common parameters.

$P_{objective}$	C_r	P_{PV}	$P_{Self\%}$
25 MW	400 kWh	10 MW	20%

Table 6. Summary of the different scenarios' results.

Scenario	Case	m	V_r	I_r	Fleet	Load L.	Objective
Base Load	Ideal	250	400	100	807	Not perfect	Best Scenario
Base Load + PV	Ideal	250	400	100	1112	Perfect	Best Scenario
Base Load + PV + Storage	Ideal	250	400	100	1106	Perfect	Best Scenario
Base Load + PV + Storage	Ideal	70	700	150	635	Perfect	Best CS/EB specifics
Base Load + PV + Storage	Real	70	700	150	350	Acceptable	Load levelling accuracy

3.2.1. Scenario without PV and Storage (Baseline Consideration)

In the first scenario the load demand before the smart charging process assumes a shape that could be that of a DN during a winter day or a DN without RDG. The transformer is over-loaded during the peak demand at noon and there is a large difference between the highest and lowest peaks. This represents a significant impact on the potential for load levelling. It is assumed in Table 5 that during the working condition without smart charging the CS assigns 100 A to each EB in order to have a low-performance CS as portrayed in Table 3. The maximum power that the CS could manage is 10 MW. In this case, the difference between the peak and the objective power is more than 10 MW, therefore the CS is not able to achieve a proper load levelling (a straight characteristic representing constant demand). In real conditions, the CS would absorb a variable power even with the I_r imposed to each EB because the number of vehicles in the CS would not be always m. It is expected that with a real fleet size the result would be worse because the difference between the power $P_{r(cs)}$ of a CS charged with I_r and the power $P_{s(cs)}$ with smart current I_s should be lower, so there should be less power available for the ancillary service. The only case that might achieve the objective is to not limit the $P_{s(cs)}$ lower boundary (0 MW), in that case the power will be negative so the vehicles will deliver power to the network. However this is not possible with the unidirectional smart charging, but easily adaptable in the algorithm. It just depends on the associated charger technology. In the analysis presented, the technology is related to a current controlled DC/DC Buck The current follows anti-symmetrically the load's behavior as expected, with a complete shut down of the CS during the noon's peaks and an over-load of 120% of the I_r during the morning demand valley. This is useful information because it was expected that for proper load levelling, the CS would absorb less current during the highest load peaks and more current during the load valleys, which is why an anti-symmetrical behavior in relation to the initial load shape is a first validation of the algorithm's efficacy. In the first scenario, the applicable fleet size is 807 in order to achieve perfect load-leveling. During the valley (0–6 a.m.), the CS will absorb up to 125% of the rated current. However, during peak demand hours at midday, the CS will not absorb current in order to achieve the load levelling. This has resulted in a large imbalance in the connection schedule, with no vehicles connected between 10 a.m.

and 5 p.m. because they are not charging. In conclusion, in a base-line scenario, without the support or benefit of PV capacity, it would be preferable to assign two different, less restrictive peak and valley shaving objectives, rather than a single load-levelling objective.

3.2.2. Scenario with PV

In the scenario that includes the PV generation, it is assumed that the PVs are working at normal operation during a sunny day, with the generated power proportional to the insulation. The load levelling appears to be achieved in this scenario. This is because the PV production creates the typical duck curve, and as a consequence, the noon peak is greatly attenuated. The power difference between the peaks is also reduced as the CS is able to remain engaged during the demand peaks. Therefore in such a scenario it is possible to assign the load levelling task to the CS without compromising the charging process. In respect to the EB charging current and SoC% considerations, it is possible to appreciate the positive effects of the PV's introduction. The main difference between Sections 3.2.1 and 3.2.2 is that the current is no longer zero at noon. With the PV scenario the CS has two peaks of overload during the 24 h, with the second one proportional to the PV power installed in the DN. The overload during the night time is unchanged. It is possible to appreciate a relatively homogeneous distribution of EBs when compared with Section 3.2.1. However the fleet necessary to actuate the load levelling with PV requires 1112 vehicles in the ideal case. In this example, the fleet is larger than in the previous case since EBs are charged (slowly) during the noon hours, thus even if the performance of the load levelling is higher, more EBs are required to do it. As a result, if the actual fleet size is smaller than the ideal one, greater care is required during the connection allocation. Moreover, the greater the difference between the "ideal" and "real" scenarios, is the greater the risk for not achieving accurate load levelling/peak shaving.

3.2.3. Scenario with PV and Storage

In the last scenario, it is assumed that the PV generation is fully engaged (100% of their rated power, so a sunny day) and that 20% of P_{PV} is stored as self consumption. The relative load behavior before the load-levelling and the PV production is represented in Figure 11 and in Figure 12 are depicted the algorithm's results relatively to the final regulated demand and the CS. Compared to Section 3.2.1, in Figure 11 it is possible to appreciate the addition of the night self-consumption, and the decrease in the PV power capacity available to reduce the demand. This has some effects on the initial demand. Firstly, the load peak is reduced during the noon period and the night load's valley depth is increased. With this DN 's scenario it is possible to achieve a full load levelling; therefore, both scenarios are suitable for such service. The corresponding currents are pictorially represented in Figure 13.

The graph Figure 12 describes:

- The red line reflects the demand without smart charging;
- The blue line reflects the demand when the CS enables the smart charging;
- The green line highlights the PV production;
- The light blue line indicates the self consumption;
- The purple line indicates the CS's absorbed power without smart charging;
- The yellow line indicates the CS's absorbed power with smart charging.

The x axis of the current map Figure 13 represents the number of EB charging slots, while the y axis represents the time in hours for a 24 h day. The charging current of each EB is represented by a small colored square 1 with a gradient that reflects the size of the charging current. Each EB's slot is represented by a square in the color map, and the current level by a different color. During a time step i, the squares have a consistent color since every vehicle is charged with I_s, save those that are practically fully charged. If the vehicles were charged with Is, their SoC would exceed the 80% SoC level, hence their current (I_e) is automatically regulated in order to achieve $SoC = 80\%$.

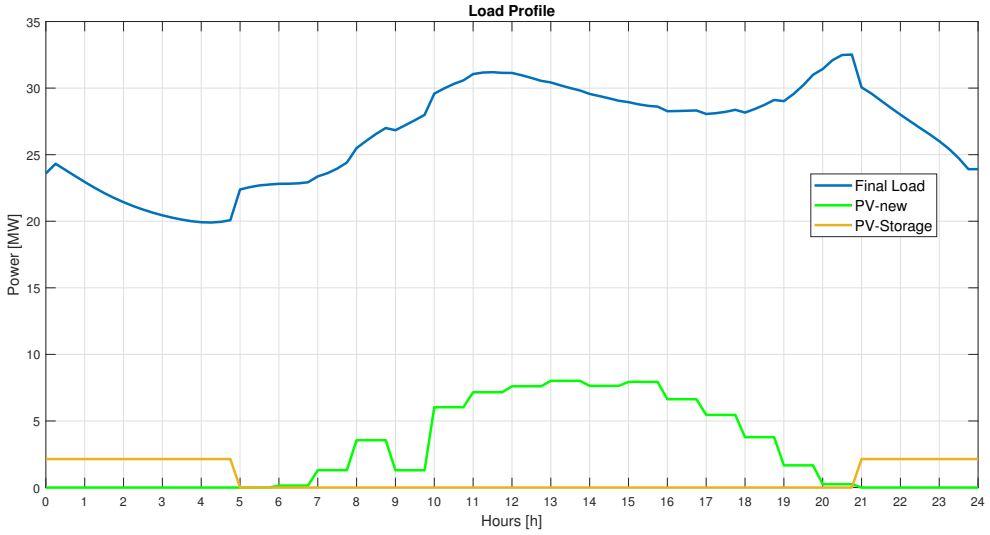

Figure 11. Demand with PV and storage.

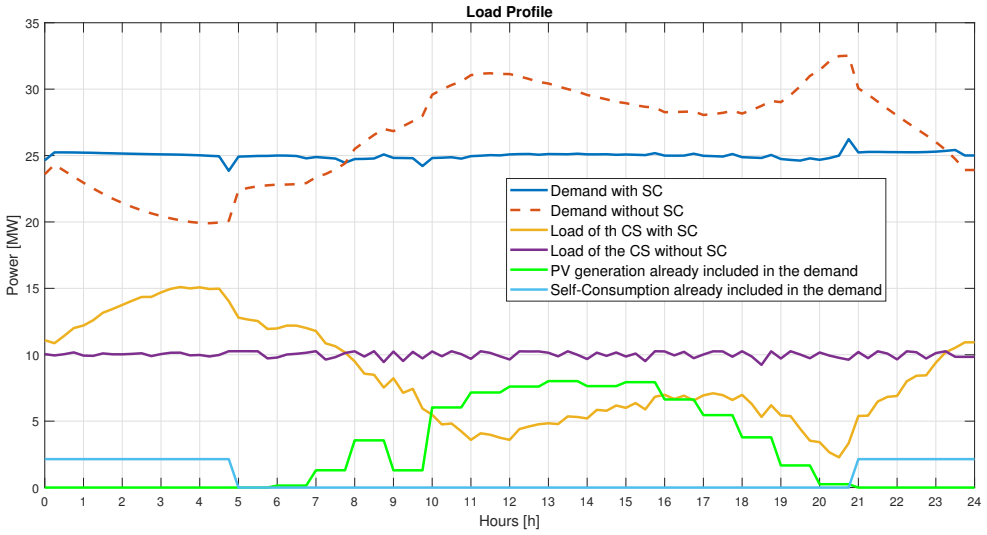

Figure 12. New demand with PV and storage.

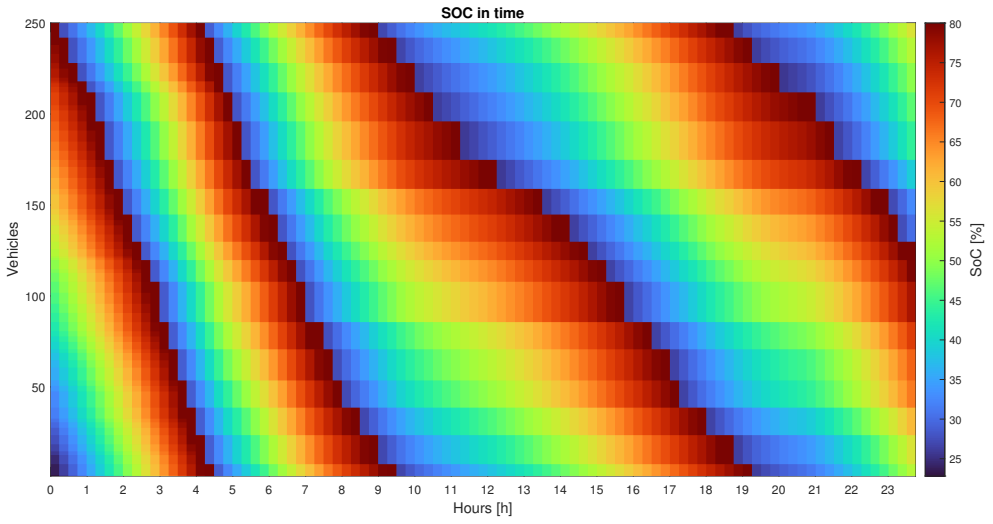

Figure 13. Smart current with PV and storage.

The current absorbed by the EBs is better balanced during the noon's hours because PV's power is reduced. On the other hand it is possible to notice that, in Figure 13, the current during the night hours is increased by 150% rather than the previous 120%. This is because the initial demand moves away from the normal demand due to the night self-consumption. The connection distribution represented in Figure 14 shows that a total fleet of 1106 EBs is required.

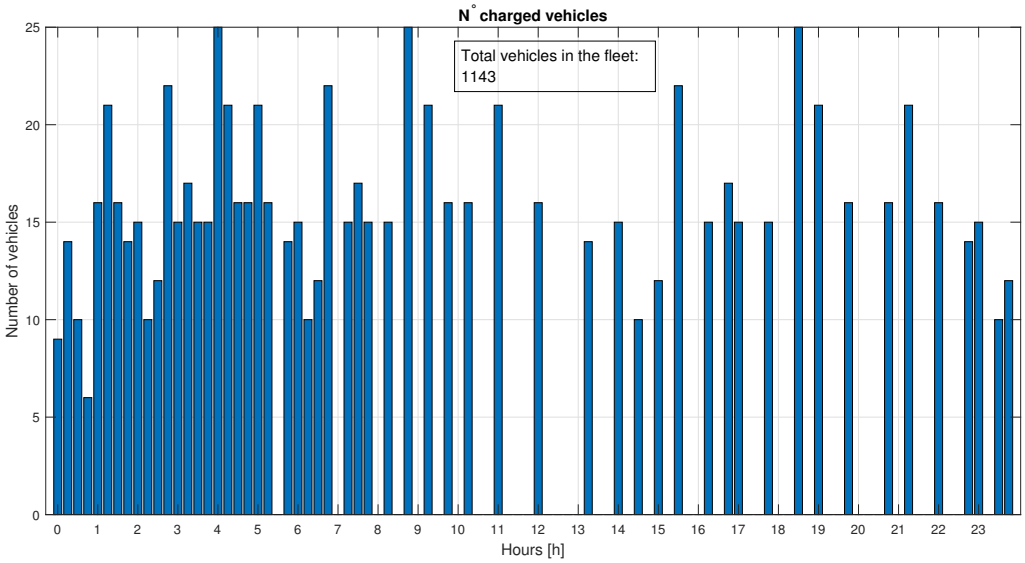

Figure 14. Connection with PV and storage.

Even if the charging current is restrained during the noon period, during the night hours, the number of EBs that are not charged during the day, are charged and connected faster during the night.

3.3. Real Scenario

Finally, the method may be used to check how the EBs must be charged and exchanged under various DN and CS situations. The final possibility is the most intriguing and should be investigated. It enables the construction of the CS and EB patterns while keeping in mind that the DN is evolving in that direction (storage and RES). The goal is to test various voltage, current, and the number of charging slots m to determine which configuration is the best when considering the F_{ideal}, the difference between $\mathbf{P}_{newload}$ and $\mathbf{P}_{objective}$. Because the graphical interpretation is not strict, the load levelling achievement is evaluated by computing the Root-Mean-Square of the error computed at each time step i with Equation (24), which assigns a value to Table 7.

$$Error = RMS(\mathbf{P}_{newload} - \mathbf{P}_{objective}). \tag{24}$$

Table 7. Numerical allocation of the load levelling graphical error.

	Load Levelling
$Error > 1$	Not Perfect
$0.3 < Error < 1$	Not Perfect during the peaks
$Error \leq 0.3$	Perfect

As the problem in this scenario involves three variables, it is challenging to create a graph with two outputs to determine which combination minimises the F_{ideal} and the error.

In addition to improving the CS and fleet parameters, it is useful to check where the Volvo's Table 4 ranks in terms of performance. Assuming that Volvo's parameters are designed to be ideal, it might be used as a test to validate the algorithm's accuracy. If the

chosen inputs yield more performant outcomes that are comparable to the Volvo's, this might be used to demonstrate the algorithm's usefulness.

Several attempts involving the PV with self consumption scenario are reported in Table 8. The table can be used to deduce information on how the DN responds to changes in the CS settings. It is possible to see that CS with fewer m charging slots results in a limited amount of EBs being required in the fleet. As a result, it is feasible to conclude that a large CS (in terms of charging slots) is not required to achieve the best results. A high charging voltage allows the CS to maintain a restrained peak of the smart charging current (within the limits presented in Table 3), while maintaining a high absorbed power (to be effective for load levelling). The test with the minor error on load levelling (0.3) was chosen as a reference because it is expected to increase when a real fleet (less than 635 EBs) is used. As a result, a working margin is established and the best scenario is defined as $V_r = 700$ V, $I_r = 150$ A, and $m = 70$. Since the extracted parameters match those in Table 4, the algorithm's functioning is validated.

Table 8. CS input parameters test.

$C_r[kWh]$	m	$V_r[V]$	$I_r[A]$	F_{ideal}	Error
400	250	400	50	614	0.6
400	250	300	50	529	1.1
400	250	300	100	864	0.3
400	50	400	100	228	2.1
400	50	500	200	404	0.6
400	50	600	300	754	0.3
400	50	600	200	488	0.4
400	50	700	200	582	0.3
400	50	700	100	306	1.2
400	50	700	150	427	0.6
400	70	700	150	635	0.3
400	70	700	100	432	0.6
400	60	700	150	532	0.3
400	55	700	125	404	0.7

The vehicles depicted in Figure 14 are unquestionably impractical in a real world context. It is not able to adjust the fleet size based on the DN's daily needs. As a result, the F_{real} constraint is applied to the most convenient scenario (using the error as a reference) from Table 8. It was decided on a $F_{real} = 350$ by considering the whole fleet of buses in Dublin [43], when the real fleet is used, as expected, the inaccuracy on load levelling grows to 0.6, which is acceptable except for some minor inaccuracies on the greatest peaks. In this case, the total fleet size is more than 1000 vehicles, with garages that can host from 70 to more than 200 vehicles spread throughout the Dublin area. It is reasonable to assume that a charging station with 70 charging slots and a small fleet of 350 EB's are values consistent with real-world data. The under-sizing of the provided values allows for a more conservative approach. As a result, it is important to work with Figure 15, which shows how many vehicles must be attached at each time step (orange). The orange bars over the blue bars reflect the number of EBs that can be allocated when the fleet size is constrained and fixed. In this scenario, uniform allocation was employed; however, different criteria can be used to assign vehicles as long as they are less or equal to the ideal requirements $z'_i \leq z_i$. As a result, it is possible to appreciate how the application of the real fleet size changes the curve from that presented in Figure 12 to the curve provided in Figure 16.

When compared to the ideal scenario, the new demand is not adequately levelled throughout the most impactful peaks and dips. However, the error increased from 0.3 to 0.6, therefore if a value with a lower F_{ideal} and $Error = 0.6$ from Table 8 was chosen, the error (and thus the final demand's shape) would be worse when the realistic fleet was applied. The CS's load without smart charging (purple) from Figure 16 is no longer constant because

the number of vehicles in the CS could be smaller than m at any time. Nonetheless, because the difference between the purple and yellow (CS load with smart charging) has an effect on demand rather than the number derived, the service can be provided.

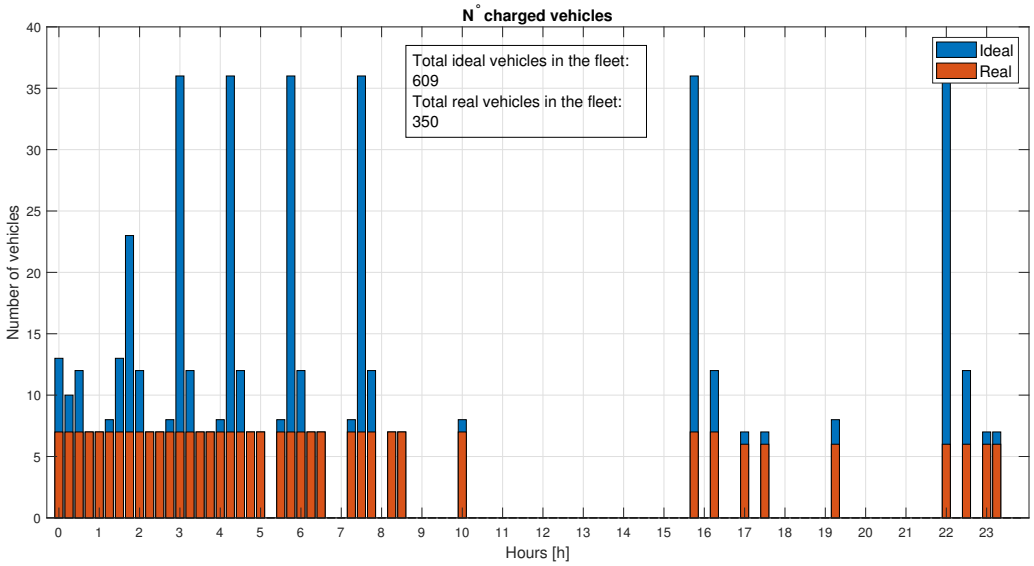

Figure 15. Real connection with PV and storage.

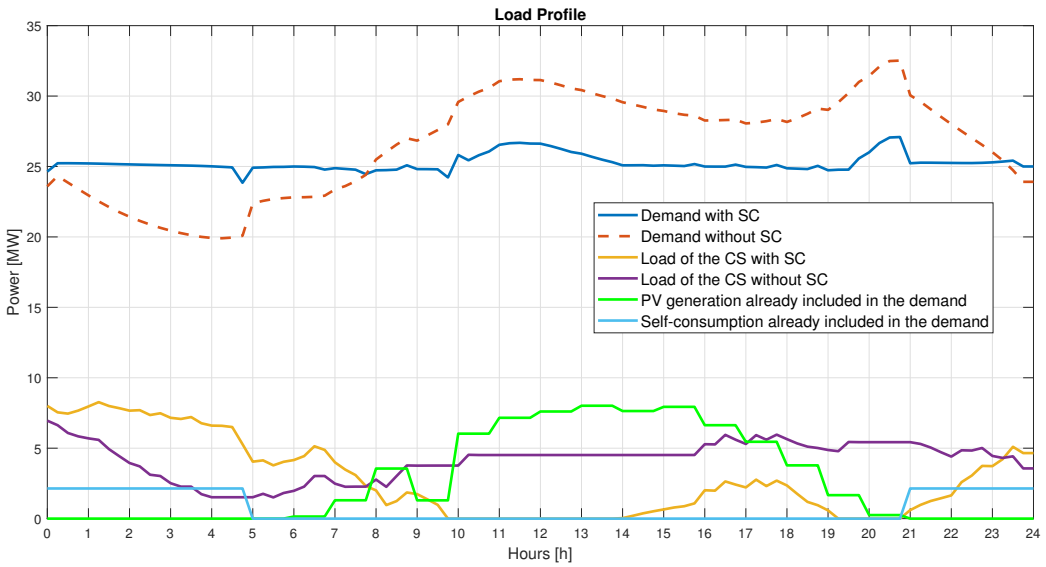

Figure 16. New real demand with PV and Storage.

There may be a considerable variation between Figures 13 and 17, which compare the current flows between the ideal and more realistic scenarios. There are many dark blue rectangles in the real arrangement that represent automobiles with $I_s = 0$. The algorithm perceives them to be fully charged connected vehicles. However, they could be disconnected in order to begin their mission. In an ideal world, when an EB is released from the CS, it is replaced by another released one. The incoming and outgoing EBs are disconnected in the real arrangement. This allows us to consider that the algorithm does not require m vehicles to be connected, which is less expensive and more practical. The same idea can be seen in Figure 18 by the rectangles with red color, which represents the three fully charged vehicles that are virtually connected but do not need to be physically connected because they are ineffective in terms of energy. The algorithm counts them as linked until they can be connected, which is why they can be disconnected, in this case since the completely charged state is decoupled by the connection one.

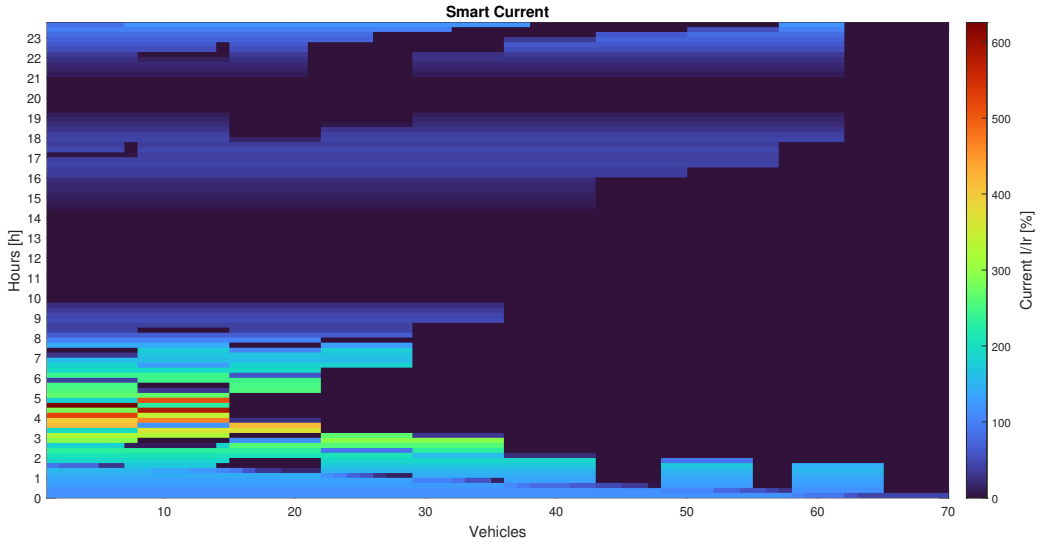

Figure 17. Real current with PV and storage.

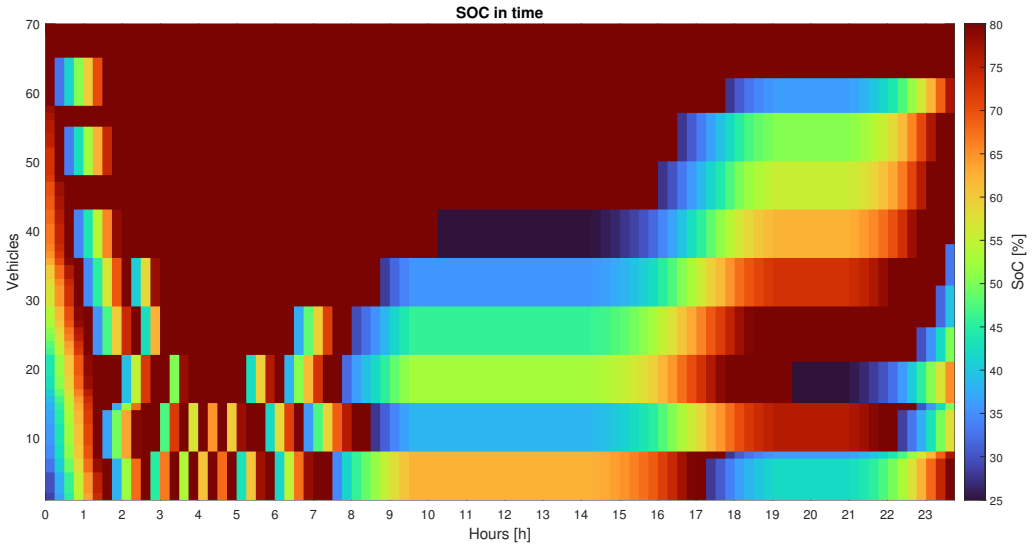

Figure 18. Real *SoC*% with PV and storage.

In addition to the introduction of the "realistic" size of the EBs fleet F_{real}, the data used initially are anticipated by the DN in the DAEM, so they may not be completely reliable. As a result, to appreciate the final demand at the main transformer, it was important to analyze how the DN responds when the CS absorbs the computed power, but with the true demand of the after-effect. This situation is examined in Figure 19, where the dashed lines represent the predicted scenario and the continuous ones represent the actual shape. The error computed with Equation (24) shows that, even if the process was investigated in the most favourable case (PV+Storage), the information on which the whole algorithm is based comes from an aleatory source, and hence the quality of the load levelling is related to the demand accuracy in the DAEM. The error produced in this case is 1.3744.

3.4. Power-Flow

As the study provided herein is predicated on the consideration of the demand at the primary transformer, the effects on the nodes and lines cannot be determined using the algorithm's results alone. In other words, a study of the impacts created by the CS demand is required to gain an appreciation of the situation and determine whether it is viable to connect this load to the DN without introducing significant compromises in terms of over/under-voltage and system losses. As a result, a NEPLAN^{TM} study on an

11-Node feeder inspired and adapted from a CIGRE benchmark of a typical European radial DN [44], as in Figure 20 with different sorts of loads in Table 9, such as commercial and residential were developed in order to have variation in active and reactive absorbed power. The lines characteristics in Table 10 and the transformers in Table 11. The non labeled arrows represent the commercial and residential loads, the labeled ones represents the PV generation and the black arrow is the CS.

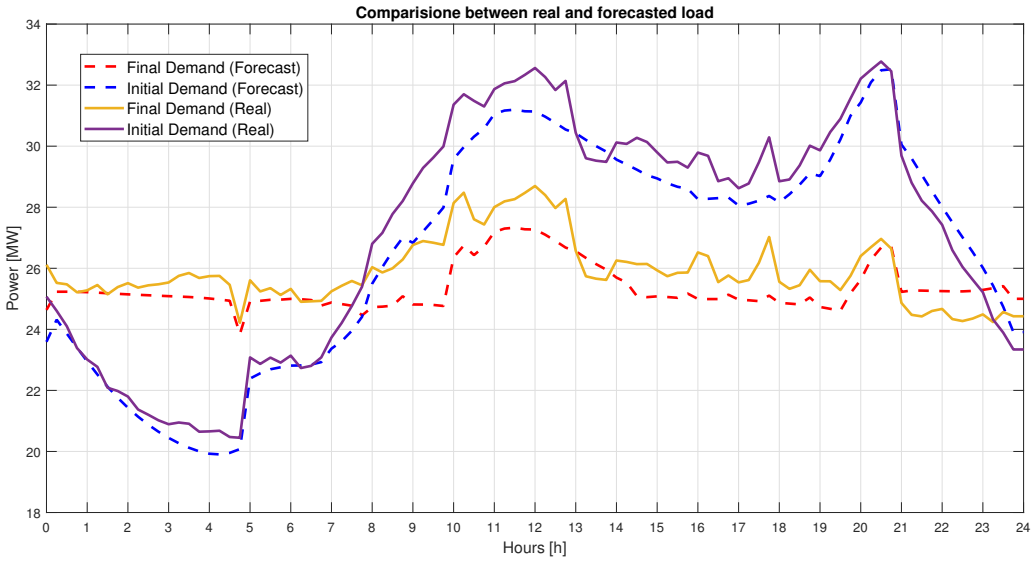

Figure 19. Comparison between forecasted and real demand.

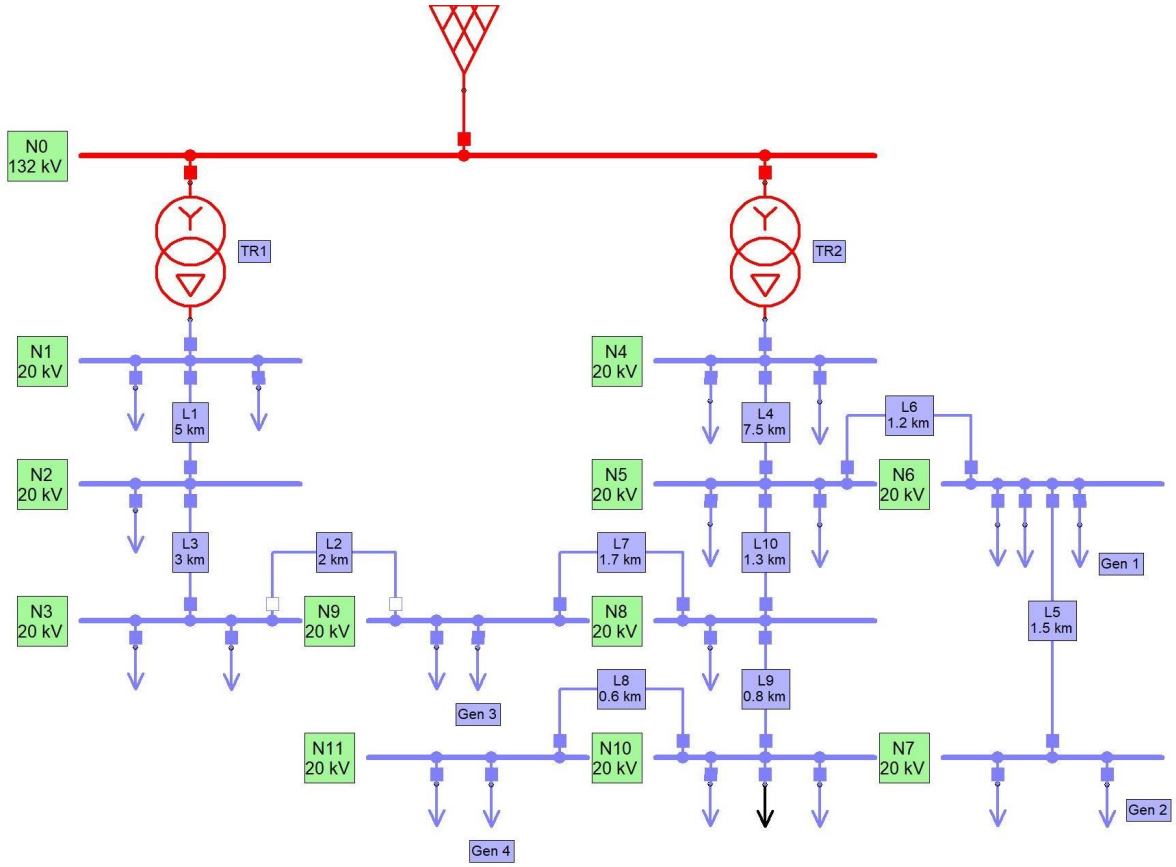

Figure 20. Eleven-Node Feeder.

Table 9. PV and loads data.

Node	S_n Res.	$\cos\varphi_R$	S_n Comm.	$\cos\varphi_C$	S_n PV	$\cos\varphi_{PV}$
	$[MVA]$		$[MVA]$		$[MVA]$	
1	9	0.98	3	0.98		
2			1.5	0.85		
3	4	0.97	1	0.85		
4	8	0.98	2	0.98		
5	0.98	0.97	1.225	0.85		
6	1.552	0.97	1.150	0.85	4	1
7	2.067	0.97			4	1
8	2.067	0.97				
9			0.5	0.85	4	1
10	1.687	0.97	1.460	0.85		
11	1.172	0.97			4	1

Table 10. Data lines.

Line	L	r	x	C	I_n
	[km]	[Ω/km]	[Ω/km]	[μF/km]	[A]
1–2	5	0.55	0.37	0.015	210
3–9	2	0.35	0.28	0.15	250
2–3	3	0.55	0.37	0.015	210
4–5	7.5	0.35	0.28	0.15	250
6–7	1.5	0.35	0.28	0.15	250
5–6	1.2	0.35	0.28	0.15	250
8–9	1.7	0.35	0.28	0.15	250
10–11	0.6	0.35	0.28	0.15	250
8–10	0.8	0.35	0.28	0.15	250
5–8	1.3	0.35	0.28	0.15	250

Table 11. Data transformers.

Nodes	Primary	Secondary	v_{cc}	p_{cc}	S_n	m
	[kV]	[kV]	[kV]	[%]	[MW]	
0–1	132	20	12	0.1	25	1
0–4	132	20	12	0.1	25	1

The active power of each load and PV is adjusted, with the coefficients explained in Table 12, in accordance with Figure 21 to achieve the same demand as shown in Figures 11 and 12.

Table 12. Load coefficients legend.

K_c	Blue	Commercial
K_r	Orange	Residential
K_{pv}	Yellow	PV
k_{cs}	Purple	CS

In this case study, the CS was connected to each node of the Feeder in Figure 20 to determine which node is the most reasonable in this circumstance. Sensitivity was assessed using the worst voltage drop or over voltage, as well as the peak of the line reactive and active losses. As seen in Table 13, where each connection is summarized with the relative effects on the worst node and losses, the best nodes are those at the secondary of the

two primary transformers. In this example, the PV production is not as incisive (the self-consumption is modelled as a reduction in commercial/residential loads), and a compete line change is not a practical degree of freedom; but, if the PV output is enhanced, the CS's connection can be moved to further nodes. The key factor influencing the predicted active power is line losses. The reactive power absorbed by the loads and lines, on the other hand, is not adjustable with the suggested method, implying that the form and magnitude are uncontrollable. The scenario in this case is the one with PV and storage, with the CS and EBs characterized 70 m charging slots with a Fleet F_{real} of 350 EBs, thus close to the Volvo data and the fleet size of a typical Dublin EB. The automated voltage of the primary feeder and the tap-changers on the primary transformers were activated in the power-flow simulation.

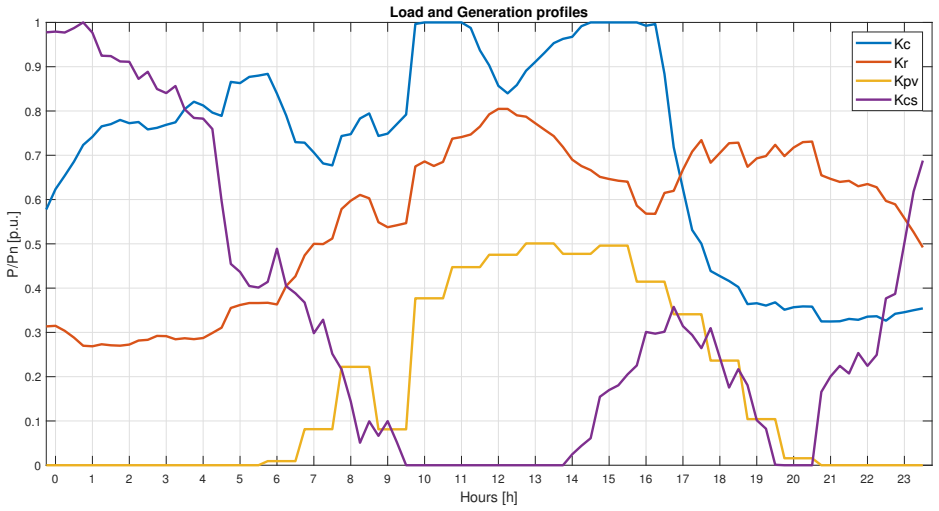

Figure 21. Load coefficients.

Table 13. Summary of the performances by changing CS's node.

CS Position	N1	N2	N3	N4	N5	N6	N7	N8	N9	N10	N11
Worst Node	N1	N3	/	N1	N1	N1	N1	N1	N1	N1	N1
Voltage %	103%	94.46%	/	103%	107%	107%	107.50%	109%	109%	109%	109.50%
Max Qloss [Mvar]	1.7	1.9	/	1.7	2.4	2.5	2.6	2.5	2.5	2.5	2.5
Max Ploss [MW]	0.6	0.8	/	0.6	1.4	1.5	1.7	1.5	1.7	1.6	1.7

Each DN's node has a minimum drop voltage of 95% and a maximum over voltage of 105% of the rated voltage (Figure 22, where are depicted the voltage of the most sensible nodes).

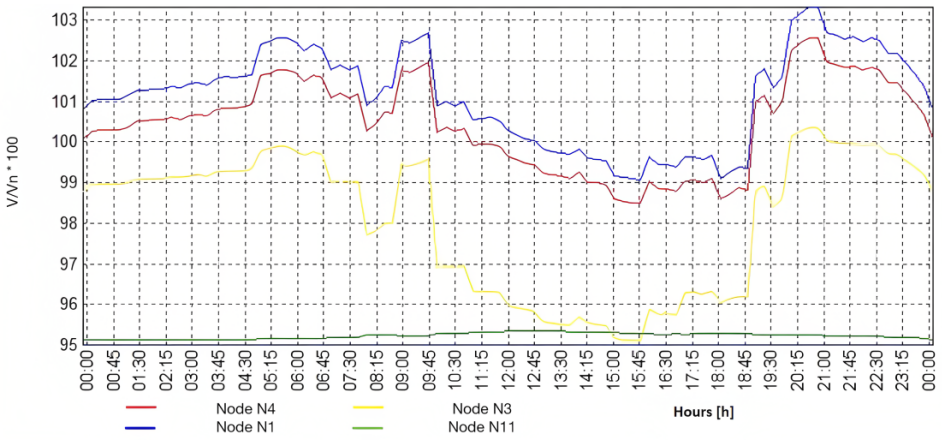

Figure 22. Voltage profile at sensible nodes.

Power losses on the line are uncontrollable and amount to about 6% of total absorbed power (Figure 23).

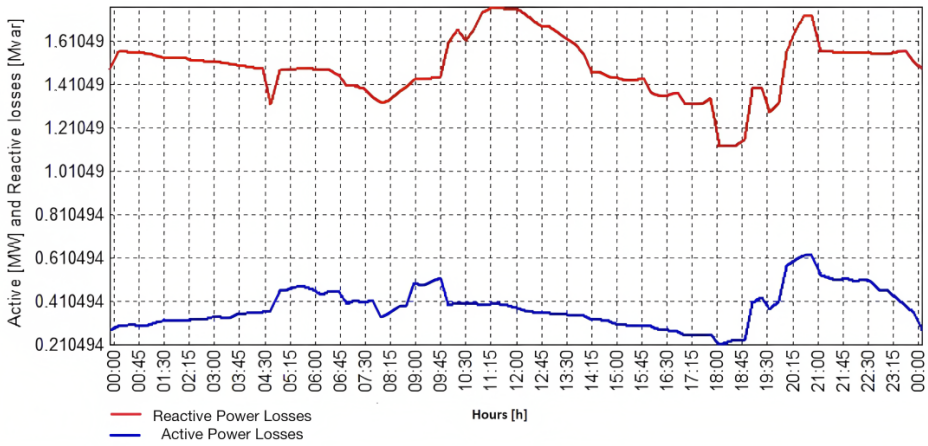

Figure 23. Power line losses.

Since the commercial loads in Table 9 have a low cos φ, the reactive power absorbed by the loads is not trivial, especially given that CS employs DAEM as a reference, which does not account for reactive power (Figure 24).

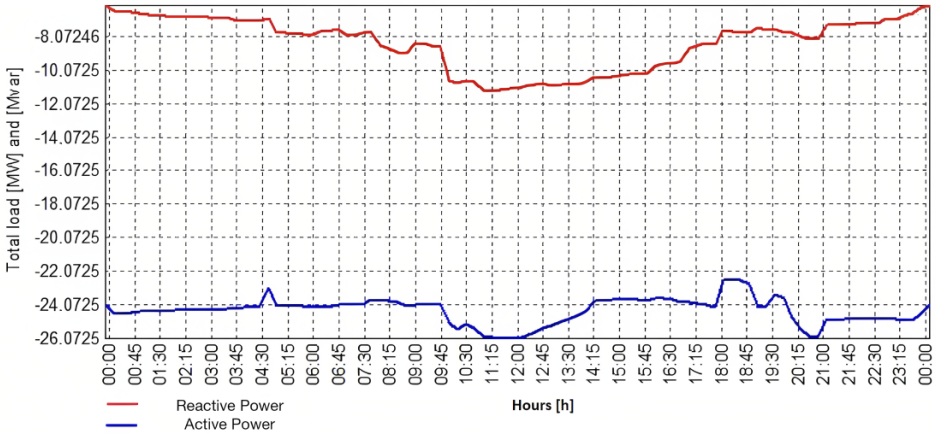

Figure 24. Active and reactive power at feeder node

In general, the effect of load levelling on active power is satisfactory. However, it deviates from the algorithm's prediction by the amount of active line losses. The largest severe impact is from unmanaged reactive power (losses and loads), although the DSO actually imposes a limit on the cos $\varphi = 0.95$ (which will increase in future). Furthermore, in the context of RDG, the inverters must be set to cos $\varphi = 1$ until the distributed reactive power controls are available.

4. Discussion

The first aspect that has a considerable impact on the charging pattern of the EBs is the demand shape. Table 5 considers a case study with approximately 1/3 of the production supplied by renewable RDG (PVs) during daylight hours, as well as self-consumption. When only PV production is considered, the net demand has the shape of a standard "duck curve". The self-consumption eventually reduces demand during low-demand periods. Even if self-consumption storage reduces the peak of PV production marginally, the end result is a net-demand that is noticeably non-uniform. This non-uniformity causes power cost imbalances, DN instability, and high start-up costs for turning on/off heat generators, and it may also damage the electrical system at the Transmission Network (TN) level [4].

As demand refers to the primary transformer that connects the DN to the TN, an increase in DN demand has mutually beneficial impacts at both levels. If it is expected to provide a full load levelling function, as shown in Table 5, the correlations mentioned in Equation (16) become more significant. When the disparity between net-demand and desired demand grows, the CS response must become more acute. The smart current I_s will increase during lower peak-hours and decrease during higher peak-hours.

During peak hours, it is vital to avoid using more power than the CS can handle because the reduction in absorbed energy by the CS may not be sufficient to meet the requirements (Equation (12)). As indicated by Equation (23),the load levelling process will not obtain the target power $\mathbf{P}_{objective}[i]$ in those time frames. The CS will no longer absorb current, therefore its power $\mathbf{P}_{s(cs)}[i]$ in those time spans will be zero (Equation (23)); the result will be not charging the EBs during this time, which may be considered unsatisfactory if this occurs on a regular basis.

The goal of making the new demand equal to the expected load (Equation (26)) may be readily fulfilled in a reverse power-flow scenario, but such a facility will allow the EBs to discharge, which is outside the scope of the presented work. If the goal is to completely achieve load levelling, a CS with more charging locations m is required. Alternatively, focus on the demand side by increasing PV production (if the peak is during the day) or self-consumption (if the peak is during the night).

$$\begin{cases} \mathbf{P}_{s(cs)}[i] = 0 \\ \mathbf{P}_{newload}[i] = \mathbf{P}_{load}[i] - (\mathbf{P}_{r(cs)}[i] - \mathbf{P}_{s(cs)}[i]) \end{cases} \tag{25}$$

$$\mathbf{P}_{newload}[i] = \mathbf{P}_{objective}[i]. \tag{26}$$

When there are significantly lower peak-hours, the CS will begin to absorb more smart current I_s in order to meet the $\mathbf{P}_{objective}[i]$. In the suggested approach, Equation (26) is always attained, although there may be some constraints that must be considered. When the $\mathbf{P}_{newload}[i] \ll \mathbf{P}_{objective}[i]$ is reached, the algorithm will iterate by adding 0.1 A to I_s until it reaches the condition specified in Equation (15). If the difference in Equation (15) is too large, the method will take a long time to converge. If the convergence time is met, the final magnitude of I_s may be insurmountable for the converters or securely supported by the batteries. A feasible approach would be to set a maximum (I_s). As in Equation (25), this will result in a limit on the CS to satisfy the load levelling service. If the goal is as specified in Equation (26), and no constraints are imposed on I_s, it should be essential to increase the F_{real}. This will distribute the requested power among more vehicles by lowering the magnitude of I_s to an acceptable level.

When the ultimate outcome, as shown in Figure 16, is examined, it is clear that the difference between the power absorbed by the CS (by imposing the rated current I_r to each EB) and the charging power facilitated by smart current I_s has an impact. As a result, it is not the magnitude of the power with EBs charged with the rated current $\mathbf{P}_{r(cs)}$ and the power with smart current $\mathbf{P}_{s(cs)}$ that influences final demand, but their difference Equation (25).

The OppCharger [41] could enable a fast and automatic exchange that is initiated when the EB is parked, allowing an electrical connection to be made in a reasonably short period if the mission is properly timed and there are no downsides. The switching timetable generated from Equation (20) only tells the time when the new EB must begin charging, not their mechanical connecting time. As a result, the EBs"in-coming' planning might be defined as anticipating the mechanical connection time to have some margin before an electrical connection. When vehicles reach the $SoC = 80\%$ Equation (17) and are still not connected out, the algorithm allows them to be viewed as being connected with an $I_s = 0$ state. As a result, they could be considered "virtually" connected, but they could also predict the disconnection and begin their mission.

Finally, the algorithm simultaneously accomplishes load levelling and smart charging of the EB without significant sacrifices. When contrasted with the $\mathbf{P}_{load}$ plot, the power

absorbed from the CS will naturally take on a mirrored shape. This indicates that the CS will absorb less power during higher peaks when the electricity price is higher, and vice versa. This will not ensure that EB charging is prioritized economically. However, when considering the behavior of $\mathbf{P}_{r(cs)}$, which only charges the EBs with rated current, the proposed smart charging will produce more economical outcomes. Because public services, such as EB transportation, are characterized by incentives and rewards [45], there is potential for a reward system based on the daily quality of the load levelling/peak shaving sought.

The method might be employed in two ways: the first is for the construction of a CS to meet DN's requirements; in this case, the parameters of the CS and EB must be set by trial and error to discover the condition that best approached the aim. The second modality takes the EB and CS parameters as input to test the effects of an existing system on various DN scenarios. In the study, both methodologies are illustrated in Sections 3.2.1–3.2.3 the test of different scenarios and, in Section 3.3, the test of different CS and EBs parameters to verify which offers the best performances. In particular, it was discovered that the requirements for the CS and EB converge to market-available and regulated ones. This confirms the main goal of the paper, which is to determine the feasibility of present technology.

Finally, by mounting the CS on different DN nodes and computing the power-flow, it was feasible to see that the ideal position is determined by the lines' capabilities and the PV's penetration. In particular, if RDG is sparse, the most practical connection point is the one closest to the secondary of the main transformer as seen in Table 13. However, with greater PV, the node could be moved further. Even if the grid-side inverter does not inject reactive power since it operates at $\cos\varphi = 1$, the reactive power from the loads and lines is uncontrollable unless there is real-time control measurement, which is beyond the scope of this study. However, because the CS currently performs two functions (load leveling of the active power and managing the EBs connection schedule), it may be possible to implement additional dedicated systems such as a synchronous condenser, condenser, static Var compensator, BESS, or batteries disposed solely for fine-tuning active and reactive power [46–48]. Assuming that the inverter on the grid side is capable of decoupling active and reactive power regulation, reactive power management could be conducted separately by employing alternative control techniques in accordance with Grid Codes or Aggregator requirements. This form of control has some limitations in terms of the inverter's power capabilities [49]—the collapse of the DC voltage side when an excessive capacitive-reactive power is absorbed, [50] or stability [51]. Therefore, the study assumes a working state of $PF = 1$ in order to simplify management.

The final data outputs Equations (17) and (20) are matrices and a vector that reflect the current values that must be imposed on each EB j as well as the number of vehicles that must be connected at time step i. They might be used directly to arrange and interpret the EBs schedule if they were represented as timetables. Meanwhile, the data from Equations (21) and (22) return the quality of the load leveling/peak shaving services as well as the amount of power that the CS will absorb.

The proposed algorithm employs the demand forecast as the primary source of data; thus, if the forecast is inaccurate, the inaccuracy caused propagates to the algorithm's outputs, as shown in Figure 19. One of the primary causes of uncertainty is the influence of the DRG [52] which may differ from the predicted condition. In such a case, the algorithm will be unable to fully achieve load-levelling because it operates in a "open-loop" form, with no ability to enable ex post modifications. In addition to RDG, there could be other uncertainty factors, such as the inability or delay of the EBs connection owing to charger failures, vehicle congestion, human errors, etc [53]. However, even a holistic strategy, such as the one suggested in this paper, can produce discrete results because it provides an easy and implementable CS control method.

The transitional context imposes a trade-off between the pursuit of ideal methods that rely on unavailable technology and the use of less performant means to execute services (such as EBs charging) that must be managed in some way so as not to disrupt the DN

service. The proposed algorithm also allows for an adaptable structure by merely acting on the software side, allowing for the future introduction of alternative working modalities such as bidirectional smart charging and active/reactive power control in real time

From the perspective of DN management, there is also the chance that additional parties will participate in the ancillary service, managed directly by the DSO or an aggregator figure [54]. In a transitory context, it is not possible to coordinate all of the players connected to the same DNs at the same time (lack of smart metering, fast communication infrastructure, etc). However, in a situation where the structures cannot communicate and coordinate in real-time, this multi-player arrangement is even more critical and requires enhanced focus and action. As the suggested method takes a target power as input, the load-levelling share of the CS can be assigned in advance. A possible segmented strategy would involve only the allocation of the power quota (e.g., 10 MW to compensate at 4 a.m.) by the DSO or an Aggregator. The power that must be levelled, as determined by the management figure, might be partitioned (for example, 6 MW to CS1 and 4 MW to CS2) and thus provided to the relative participants. As a result, the proposed technique could be used in a DN with multiple participants by using a coordinator that manages the power-quota of different players. The coarse regulation using EBs might also be intended as the structure of the new load, where devices with lower capacity and higher uncertainty could gradually be introduced as fine regulation (EVs, private PV production, etc.) to achieve better load levelling.

In summary, the proposed algorithm does not necessitate a complicated communication infrastructure because it depends on DAEM data and technologies that are readily available in a municipality. However, it is not intended to be a stand-alone solution, but rather a transitional technology that may be incrementally improved until the system is ready to host the complete V2G service. Furthermore, depending on the DC/DC converter used, the CS may be reused for reverse power flow. Furthermore, it may be feasible to change the assignment of the real fleet, not only in a non-uniform distribution, but also in accordance with actual practical capability. Regarding the overall results, the suggested algorithm manages CS and EBs in an appropriate manner for a coarse regulation of the active power for a suitable management of the EB's schedule.

Future advances could include designing the algorithm, CS, and EB mutual effects so that they can be easily upgraded to real-time control systems that can account for many charging stations in the same DN and reactive power regulation. Or, at the very least, to ensure a smooth transition to more sophisticated systems, when Smart Grids will be able to properly handle the communication/control of the DN's components without changing the entire infrastructure, but only the control approach.

5. Conclusions

In conclusion, the algorithm simultaneously accomplishes load levelling and smart charging of the EB without significant sacrifices. It might be used to design the charging station as a function of the DN's total demand shape, or to test the effects of several DN scenarios on a given charging station. The output findings might be used immediately to build and read the EB's timetable, producing instruction ready for use by the CS's operators. Because the connecting node for the CS cannot be changed due to network restrictions, the position that created the less acute effects (line losses and node voltage drop) can be relocated away from the primary node in proportion to the installed power of the PV. However, even though real-time sophisticated communication and control systems are not used, the compatibility of a high-capacity CS is consistent with the eventual penetration of RDG in the DN. The limits originate from the unreliability of DAEM data and the inability to manage reactive power, which might be delegated to other specified systems. In summary, the proposed algorithm does not necessitate a complex communication infrastructure, and it is not intended to be a stand-alone solution, but rather a transitional technology that can be incrementally modified until the system is ready to host the V2G service entirely. Future work may concentrate on the algorithm's scalability for future technological settings or

on enhancing the design to appropriately house them, as well as to control additional CS or electrical users connected to the same DN in order to correctly assign the load-leveling effort, based on the available EBs.

Author Contributions: Conceptualization, N.D.; methodology, N.D.; software, N.D.; validation, K.S., R.T. and F.B.; formal analysis, K.S., R.T. and F.B.; investigation, N.D.; resources, N.D. and R.T.; data curation, N.D., K.S. and R.T.; writing—original draft preparation, N.D.; writing—review and editing, K.S.; visualization, F.B.; supervision, R.T. and K.S.; All authors have read and agreed to the published version of the manuscript.

Funding: This research received no external funding.

Institutional Review Board Statement: Not applicable.

Informed Consent Statement: Not applicable.

Data Availability Statement: The data presented in this study are available on request from the corresponding author.

Conflicts of Interest: The authors declare no conflict of interest.

Abbreviations

The following abbreviations are used in this manuscript:

CS	Charging Station
$\mathbf{P}_{r(CS)}$	CS Power vector with I_r
$\mathbf{P}_{s(CS)}$	CS Power vector with I_s
DAEM	Day Ahead Energy Market
$\mathbf{Cnn}_{real}$	EB's real connection schedule vector
Cnn	EB's connection schedule vector
EB	Electric Bus
EV	Electric Vehicle
ΔE_{CS}	Element of $\mathbf{E}_{load}$ vector
$\mathbf{E}_{load}$	Energy difference vector
$E[Wh]$	Energy in [Wh]
$E_{j(r)}$	Energy of EB j charged with I_r
$E_{j(s)}$	Energy of EB j charged with I_s
$\mathbf{P}_{newload}$	Final New DN's demand after smart-charging
$\mathbf{P}_{load}$	Initial Demand power vector
Is	I_s Matrix
m	Number of EBs in the CS
z	Number of fully charged EBs
z'	Number of connected EBs in the real case
$\mathbf{P}_{objective}$	Objective Demand power vector
PV	Photovoltaic
C_r	Rated Capacity
I_r	Rated current
V_r	Rated Voltage
RDG	Renewable Distributed Generation
F_{ideal}	Size of the ideal EB's fleet
F_{real}	Size of the real EB's fleet
SC	Smart Charging
I_e	Smart current for almost-charged vehicles
I_s	Smart current
SoC	SoC Matrix
SoC	State-of-Charge
i	Time-step index
Δt	Time-step
j	Vehicle index

References

1. Global Electric Car Stock, 2010-2021-Charts-Data & Statistics-IEA. Available online: https://www.iea.org/data-and-statistics/charts/global-electric-passenger-car-stock-2010-2020 (accessed on 10 September 2022).
2. Net Zero Coalition | United Nations. Available online: https://www.un.org/en/climatechange/net-zero-coalition (accessed on 27 May 2022).
3. Da Silva, E.C.; Melgar-Dominguez, O.D.; Romero, R. Simultaneous distributed generation and electric vehicles hosting capacity assessment in electric distribution systems. *IEEE Access* **2021**, *9*, 110927–110939. [CrossRef]
4. Wong, L.A.; Ramachandaramurthy, V.K. A Case Study on Optimal Sizing of Battery Energy Storage to Solve 'Duck Curve' Issues in Malaysia. In Proceedings of the 2020 8th International Conference on Smart Grid and Clean Energy Technologies (ICSGCE 2020), Kuching, Malaysia, 4–7 October 2020; pp. 1–4. [CrossRef]
5. Xie, Z.; Qi, W.; Huang, C.; Li, H. Effect Analysis of EV Optimal Charging on DG Integration in Distribution Network. In Proceedings of the 8th IEEE International Conference on Advanced Power System Automation and Protection (APAP 2019), Xi'an, China, 21–24 October 2019; pp. 525–528. [CrossRef]
6. Song, X.; Yuan, H.; Xiaoxuan, Z.; Jing, L.; Li, M. Evaluation Model for World-Class Distribution Network Management. In Proceedings of the 2018 China International Conference on Electricity Distribution (CICED) 2018, Tianjin, China, 17–19 September 2018.
7. Iclodean, C.; Varga, B.; Burnete, N.; Cimerdean, D.; Jurchiş, B. Comparison of Different Battery Types for Electric Vehicles. In Proceedings of the IOP Conference Series: Materials Science and Engineering, Pitesti, Romania, 8–10 November 2017; Institute of Physics Publishing: Bristol, UK, 2017; Volume 252. [CrossRef]
8. Yannick, P.; Marc, P.; Willett, K. A Public Policy Strategies for Electric Vehicles and for Vehicle to Grid Power. In Proceedings of the 2013 World Electric Vehicle Symposium and Exhibition (EVS27), Barcelona, Spain, 17–20 November 2013. [CrossRef]
9. Noel, L.; Mccormack, R. A Cost Benefit Analysis of a V2G-Capable Electric School Bus Compared to a Traditional Diesel School Bus. *Appl. Energy* **2014**, *126*, 246–255. [CrossRef]
10. Tremblay, O.; Dessaint, L.A. Experimental Validation of a Battery Dynamic Model for EV Applications. *World Electr. Veh. J.* **2009**, *3*, 289–298.
11. Uddin, M.; Romlie, M.F.; Abdullah, M.F.; Abd Halim, S.; Abu Bakar, A.H.; Chia Kwang, T. A review on peak load shaving strategies. *Renew. Sustain. Energy Rev.* **2018**, *82*, 3323–3332. [CrossRef]
12. Electric Car Sales Share in the Net Zero Scenario, 2000-2030-Charts-Data & Statistics-IEA. Available online: https://www.iea.org/data-and-statistics/charts/electric-car-sales-share-in-the-net-zero-scenario-2000-2030 (accessed on 10 September 2022).
13. Global EV Data Explorer-Data Tools-IEA. Available online: https://www.iea.org/data-and-statistics/data-tools/global-ev-data-explorer (accessed on 9 January 2023).
14. Nieuwenhuijsen, M.J.; Khreis, H. Car free cities: Pathway to healthy urban living. *Environ. Int.* **2016**, *94*, 251–262. [CrossRef]
15. Amietszajew, T.; McTurk, E.; Fleming, J.; Bhagat, R. Understanding the limits of rapid charging using instrumented commercial 18650 high-energy Li-ion cells. *Electrochim. Acta* **2018**, *263*, 346–352. [CrossRef]
16. Darii, N.; Turri, R.; Sunderland, K. Electric Bus Demand Management through Unidirectional Smart Charging. In Proceedings of the 2022 57th International Universities Power Engineering Conference (UPEC), Istanbul, Turkey, 30 August–2 September 2022; pp. 1–6. [CrossRef]
17. Berckmans, G.; Messagie, M.; Smekens, J.; Omar, N.; Vanhaverbeke, L.; Mierlo, J.V. Cost Projection of State of the Art Lithium-Ion Batteries for Electric Vehicles Up to 2030. *Energies* **2017**, *10*, 1314. [CrossRef]
18. Sujitha, N.; Krithiga, S. RES based EV battery charging system: A review. *Renew. Sustain. Energy Rev.* **2017**, *75*, 978–988. [CrossRef]
19. Chen, X.; Shen, W.; Vo, T.T.; Cao, Z.; Kapoor, A. An Overview of Lithium-ion Batteries for Electric Vehicles. In Proceedings of the 2012 10th International Power & Energy Conference (IPEC), Ho Chi Minh City, Vietnam, 12–14 December 2012. [CrossRef]
20. Krewer, U.; Röder, F.; Harinath, E.; Braatz, R.D.; Bedürftig, B.; Findeisen, R. Review-Dynamic Models of Li-Ion Batteries for Diagnosis and Operation: A Review and Perspective. *J. Electrochem. Soc.* **2018**, *165*, A3656. [CrossRef]
21. Zhang, X.; Zhang, W.; Lei, G. A Review of Li-ion Battery Equivalent Circuit Models. *Trans. Electr. Electron. Mater.* **2016**, *17*, 311–316. [CrossRef]
22. Gaehring, A.; Kripalani, R.; Rondeau, O.; Schlag, N. Modeling Li-ion Battery Behavior to Identify Safety Limits; Modeling Li-ion Battery Behavior to Identify Safety Limits. In Proceedings of the 2021 IEEE MIT Undergraduate Research Technology Conference (URTC), Cambridge, MA, USA, 8–10 October 2021. [CrossRef]
23. Yu, Z.; Xiaoping, C.; Yufeng, Z. The influence of coupling of charge/discharge rate and short term cycle on the battery capacity of Li-ion batteries. In Proceedings of the 2019 3rd International Conference on Electronic Information Technology and Computer Engineering (EITCE), Xiamen, China, 18–20 October 2019.
24. Wang, L.; Chen, B. Model-Based Analysis of V2G Impact on Battery Degradation. *SAE Tech. Pap.* **2017**. [CrossRef]
25. Yilmaz, M.; Krein, P.T. Review of battery charger topologies, charging power levels, and infrastructure for plug-in electric and hybrid vehicles. *IEEE Trans. Power Electron.* **2013**, *28*, 2151–2169. [CrossRef]
26. Yong Qiang, Z.; YueQiang, W.; Yuan, S.H. Energy Management of Low Voltage Power Supply of Plug-in Hybrid Electric Vehicle. *IFAC-PapersOnLine* **2018**, *51*, 1–6. [CrossRef]

27. Ullah Khan, S.; Khalid Mehmood, K.; Maqsood Haider, Z.; Basit Ali Bukhari, S.; Lee, S.J.; Kashif Rafique, M.; Kim, C.H. Energy Management Scheme for an EV Smart Charger V2G/G2V Application with an EV Power Allocation Technique and Voltage Regulation. *Appl. Sci.* **2018**, *8*, 648. [CrossRef]
28. Mohan, N.; Undeland, T.M.; Robbins, W.P.; Legoprint, L. *Power Electronics: Converters Applications and Design*, 2nd ed.; Wiley: Hoboken, NJ, USA, 1995.
29. Zhuang, P.; Liang, H. Stochastic Energy Management of Electric Bus Charging Stations With Renewable Energy Integration and B2G Capabilities. *IEEE Trans. Sustain. Energy* **2021**, *12*, 1206–1216. [CrossRef]
30. Han, B.; Liu, H.; Zhang, C.; Xue, F.; Lu, S. Electric Bus Energy Management and Routing Scheduling Considering Timetable Constraints. In Proceedings of the 4th International Conference on Power and Energy Technology (ICPET), Beijing, China, 28–31 July 2022; pp. 1058–1063. [CrossRef]
31. Hasan, M.M.; El Baghdadi, M.; Hegazy, O. Energy Management Strategy in Electric Buses for Public Transport using ECO-driving. In Proceedings of the 2020 15th International Conference on Ecological Vehicles and Renewable Energies (EVER 2020), Monte-Carlo, Monaco, 10–12 September 2020. [CrossRef]
32. Gkiotsalitis, K. Bus rescheduling in rolling horizons for regularity-based services. *J. Intell. Transp. Syst. Technol. Plan. Oper.* **2021**, *25*, 356–375. [CrossRef]
33. Zhang, C. Charging schedule optimization of electric bus charging station considering departure timetable. *IET Conf. Publ.* **2019**, *2019*. [CrossRef]
34. Torabi, R.; Gomes, A.; Morgado-Dias, F. The Duck Curve Characteristic and Storage Requirements for Greening the Island of Porto Santo. In Proceedings of the Energy and Sustainability in Small Developing Economies, ES2DE 2018, Funchal, Portugal, 9–12 July 2018; pp. 13–20. [CrossRef]
35. Farzam Far, M.; Paakkinen, M.; Cremers, P. A Framework for Charging Standardisation of Electric Buses in Europe. In Proceedings of the 2020 IEEE Vehicle Power and Propulsion Conference (VPPC), Gijon, Spain, 18 November 2020–16 December 2020. [CrossRef]
36. Trucks and Buses-Analysis-IEA. Available online: https://www.iea.org/reports/trucks-and-buses (accessed on 10 October 2022).
37. ASSURED Project Concludes and Launches Clean Bus Report-News-ASSURED Project. Available online: https://assured-project.eu/news-and-events/news/assured-project-concludes-and-launches-clean-bus-report (accessed on 6 September 2022).
38. Home-ZeEUS-Zero Emission Urban Bus System. Available online: https://zeeus.eu/ (accessed on 6 September 2022).
39. J1772_201710: SAE Electric Vehicle and Plug in Hybrid Electric Vehicle Conductive Charge Coupler-SAE International. Available online: https://www.sae.org/standards/content/j1772_201710/ (accessed on 6 September 2022).
40. Wang, B.; Member, S.; Dehghanian, P.; Wang, S.; Mitolo, M.; Member, S. Electrical Safety Considerations in Large-Scale Electric Vehicle Charging Stations; Electrical Safety Considerations in Large-Scale Electric Vehicle Charging Stations. *IEEE Trans. Ind. Appl.* **2019**, *55*, 6603. [CrossRef]
41. OppCharge-Fast Charging of Electric Vehicles. Available online: https://www.oppcharge.org/ (accessed on 29 May 2022).
42. Volvo Buses | Sustainable Public Transport Systems. Available online: https://www.volvobuses.com/it/ (accessed on 6 September 2022).
43. Dublin Bus Flee-Dublin Bus. Available online: http://www.dublinbus.ie/About-Us/Dublin-Bus-Fleet/ (accessed on 4 October 2022).
44. Conseil international des grands reseaux electriques. Comite detudes C6..; (Impr. Conformes). In *Benchmark Systems for Network Integration of Renewable and Distributed Energy Resources*; CIGRE: Paris, France, 2014.
45. Krawiec, S.; Łazarz, B.; Markusik, S.; Karoń, G.; Sierpiński, G.; Krawiec, K.; Janecki, R. Urban public transport with the use of electric buses-Development tendencies. *Transp. Probl.* **2016**, *11*, 127–137. [CrossRef]
46. Jordehi, A.R.; Javadi, M.S.; Catalão, J.P. Energy management in microgrids with battery swap stations and var compensators. *J. Clean. Prod.* **2020**, *272*, 122943. [CrossRef]
47. Fedayi, H.; Ahmadi, M.; Faiq, A.B.; Urasaki, N.; Senjyu, T. BESS based voltage stability improvement enhancing the optimal control of real and reactive power compensation. *AIMS Energy* **2022**, *10*, 535–552. [CrossRef]
48. Zhou, X.; Wei, K.; Ma, Y.; Gao, Z. A review of reactive power compensation devices. In Proceedings of the 2018 IEEE International Conference on Mechatronics and Automation (ICMA 2018), Changchun, China, 5–8 August 2018; pp. 2020–2024. [CrossRef]
49. NERC. *Power Plant Model Verification for Inverter-Based Resources*; NERC: Atlanta, GA, USA, 2018.
50. Lu, D.; Wang, X.; Blaabjerg, F. Influence of Reactive Power Flow on the DC-Link Voltage Control in Voltage-Source Converters. In Proceedings of the 2018 IEEE Energy Conversion Congress and Exposition (ECCE 2018), Portland, OR, USA, 23–27 September 2018; pp. 2236–2241. [CrossRef]
51. Li, H.; Xu, Y.; Adhikari, S.; Rizy, D.T.; Li, F.; Irminger, P. Real and reactive power control of a three-phase single-stage PV system and PV voltage stability. In Proceedings of the IEEE Power and Energy Society General Meeting, San Diego, CA, USA, 22–26 July 2012. [CrossRef]
52. Simankov, V.S.; Buchatskiy, P.Y.; Shopin, A.V.; Teploukhov, S.V.; Buchatskaya, V.V. Control of an Autonomous Energy Complex with Renewable Energy Sources, taking into account the Type of Input Information Uncertainty. In Proceedings of the 2021 4th International Conference on Control in Technical Systems (CTS 2021), Saint Petersburg, Russian, 21–23 September 2021; pp. 252–255. [CrossRef]

53. Xu, N.Z.; Chung, C.Y. Uncertainties of EV Charging and Effects on Well-Being Analysis of Generating Systems. *IEEE Trans. Power Syst.* **2015**, *30*, 2547–2557. [CrossRef]
54. Wu, H.; Shahidehpour, M.; Alabdulwahab, A.; Abusorrah, A. A game theoretic approach to risk-based optimal bidding strategies for electric vehicle aggregators in electricity markets with variable wind energy resources. *IEEE Trans. Sustain. Energy* **2016**, *7*, 374–385. [CrossRef]